# A New Method for Calculating Deflection of FRP Reinforced Concrete Beams Using the Tension Stiffening Concept

**Feras Sheitt**

Submitted to the
Institution of Graduate Studies and Research
in partial fulfillment of the requirements for degree of

Master in Science
in
Civil Engineering

Eastern Mediterranean University
September 2015
Gazimağusa, North Cyprus

Approval of the Institute of Graduate Studies and Research

Prof. Dr. Serhan Çiftçioğlu
Acting Director

I certify that this thesis satisfies the requirements as a thesis for the degree of Master of Science in Civil Engineering.

Prof. Dr. Özgür Eren
Chair, Department of Civil Engineering

We certify that we have read this thesis and that in our opinion it is fully adequate in scope and quality as a thesis for the degree of Master of Science in Civil Engineering.

Prof. Dr. A Ghani Razaqpur
Co-supervisor

Asst. Prof. Dr. Serhan Şensoy
Supervisor

Examining Committee

1. Prof. Dr. Özgür Eren

2. Asst. Prof. Dr. Giray Ozay

3. Asst. Prof. Dr. Serhan Şensoy

# ABSTRACT

Accurate calculation of the deflection of reinforced concrete members has been a challenge since the inception of modern reinforced concrete. Many formulas and methods have been developed, over the years. However, most of them are empirical in nature and do not predict accurately the flexural deflection of reinforced concrete members over the entire loading range. Deflection calculation has important impact on the satisfactory performance of structures, especially in performance based design and in the design of fiber reinforced polymers (FRP) reinforced concrete members, where deflection limits may govern the design. This highlights the need for more accurate deflection calculation methods. This research proposes a method, based on first principles, to more accurately calculate, compared to ACI Committee 440 and CSA S806-12 methods, the deflection of FRP reinforced beams. The method has two key features: (1) It accounts, via a tension-stiffening model, for the contribution of the concrete teeth between flexural cracks to the stiffness of the beam; (2) the method is developed by dividing the beam cross-section at selected points along its span into several layers. The contribution of each layer to the flexural rigidity is computed by finding its elastic modulus (secant modulus) as function of the type and magnitude of the longitudinal stress (strain) at the level of the centroid of that layer. The layers flexural rigidities are summed over each cross-section and used in conjunction with the second moment-area theorem to compute the beam deflection. This method is based on first principles and no empirical factors are involved besides the adopted tension-stiffening model. The validity of the proposed method is demonstrated by comparing its results with corresponding experimental data. It is shown that it can estimates the deflection at the serviceability load levels quite accurately. Also it is

reliable in estimating deflection under load levels beyond serviceability, which is a limitation to of both the ACI Committee 440 and CSA S806-12 methods. The proposed method was applied on steel reinforced beam and compared with experimental and ACI Committee 318 results. The proposed method gave reliable results, but further investigation for the case of steel reinforced beams is required.

**Keywords:** Deflection, FRP reinforced concrete, Flexural behavior, Tension stiffening.

# ÖZ

Betonarme elemanlarda deformasyon hesaplarının yıllardır gerçeğe yakın hesaplanabilmesi nerdeyse betonarmenin keşfi ile birlikte tartışılmaktadır. Bu konuda birçok formül ve yöntem geliştirilmiş olmasına rağmen, deneysel çalışmalar ve gözleme dayalı olmaları, farklı hesap yöntemlerinin uygulanmasına neden olmuştur. Özellikle sınır durumlar yöntemi ve performansa göre tasarımın ön planda olduğu bu günlerde, deformasyon hesaplarının etkisi artmış bulunmaktadır. Bu durum, deformasyon hesaplarındaki hassasiyeti artırmaktadır. Bu çalışma sonucu FRP donatılı kirişler için önerilen yöntem ACI 440 ve CSA S806-12 yöntemleri gibi güvenilir olarak saptanmıştır. Geliştirlen bu yöntemde, elastik modülün ve atalet momentinin efektif değerlerinin kullanılmasının yanında betonun çatlama sonrası çeki gerilmeleri de göz önünde bulundurulmuştur. Bu çalışma sonucunda ampirik bağıntılar kullanılmadan tamamen teori bazlı bir yöntem önerilmektedir. Ayni zamanda bu çalışma sonucunda önerilen yöntem kullanılarak elde edilen deformasyon değerleri mevcut deneysel çalışmalarla karşılaştırılmıştır. Tahmin edilen deformasyon değerleri, elemanlardan beklenen kullanılabilirlik sınır durumu seviyesinde kabul edilebilir seviyedeyken, bu yöntem, ACI 440 ve CSA S806-12'nin aksine kullanılabilirlik sınır durumu ötesinde de güvenilir sonuçlar vermiştir. Bu yöntem ayrıca çelik donatılı betonarme kirişe de uygulanmış olup ACI 318 ve deneysel sonuçlarla karşılaştırılmıştır. Bu yöntem ayni şekilde çelik donatılı betonarme kiriş için de güvenilir sonuçlar vermiştir ancak çelik donatılı kirişler için daha ileri seviyede detaylı çalışma gerekmektedir.

**Anahtar kelimeler:** Deformasyon, FRP donatılı betonarme, eğilme davranışı, çatlamış kesitteki çeki etkisi

# DEDICATION

To My Parents, Family, Friends, and Beloved Ones

# ACKNOWLEDGMENT

I would like to thank everyone who contributed to the achievement of this work specially my family and friends.

Moreover, I would like to thank my Supervisor Asst. Prof. Dr. Serhan Şensoy and my Co-supervisor Prof. Dr. A Ghani Razaqpur for their continuous guidance and support during the preparation of this thesis.

Also I would like to thank all of my instructors for every piece of information they taught me. Without their knowledge, I could not finish this research work and draw conclusions out of it.

Moreover, Special thanks for Dra. Cristina Barris Peña and her colleagues for the data used in the verification of the proposed method for FRP reinforced beams.

Lastly, I would like to thank Prof. Dr. Wenjun Qu and his colleagues for the verification data for steel reinforced beam.

# TABLE OF CONTENT

ABSTRACT ..... iii

ÖZ ..... v

DEDICATION ..... v

ACKNOWLEDGMENT ..... vii

LIST OF TABLES ..... xi

LIST OF FIGURES ..... xiii

LIST OF SYMBOLS ..... xv

1 INTRODUCTION ..... 1

1.1 Importance of research ..... 1

1.2 Long term vs. short term deflection ..... 2

1.3 Objective of the research ..... 2

1.4 Introduction to chapters ..... 2

2 LITERATURE REVIEW ..... 4

2.1 Introduction ..... 4

2.2 Deflection theory ..... 5

2.3 Extension of elastic deflection theory to inelastic non homogeneous beams ... 8

2.3.1 Tension stiffening ..... 10

2.3.1.1 Historical overview ..... 10

2.3.1.2 Fields of application ..... 11

2.3.1.3 Factors affecting tension stiffening ..... 11

2.3.1.4 Tension stiffening decaying ..... 12

2.3.1.5 Tension stiffening in flexural members ..... 12

2.3.1.6 Tension stiffening in prestressed concrete ..... 12

2.3.1.7 Cyclic loading ..... 13
2.3.1.8 Negative tension stiffening ..... 13
2.3.1.9 Models considering tension stiffening ..... 13
2.3.1.10 Tension stiffening relationship with reinforcement ratio ..... 15
3 PROPOSED METHOD ..... 17
3.1 Introduction ..... 17
3.2 Constitutive laws of reinforced concrete ..... 17
3.2.1 Steel reinforcement ..... 18
3.2.2 Fiber reinforced polymer (FRP) reinforcement ..... 18
3.2.3 Concrete ..... 19
3.2.3.1 Concrete in compression ..... 19
3.2.3.2 Concrete in tension ..... 20
3.3 Moment-area method ..... 21
3.4 Moment of inertia ..... 22
3.5 Effective elastic modulus ..... 23
3.5.1 Classification of cases due to the stress level in tension part of cross section ..... 25
3.5.1.1 Case I: $10c' > Y = d - c$ and $c' < Y = d - c$ ..... 25
3.5.1.2 Case II: $10\,c' < Y = d - c$ ..... 26
3.5.1.3 Secant modulus of elasticity ..... 27
3.6 Step-by-step procedure for calculating beam deflection ..... 28
3.6.1 CSA S806-12 method ..... 32
3.6.1.1 Before cracking ..... 32
3.6.1.2 After cracking ..... 32
3.6.2 ACI Committee 440.1 R-06 method: ..... 32

3.6.2.1 Before cracking ..... 32
3.6.2.2 After cracking ..... 33
4 VERIFICATION AND DISCUSSIONS ..... 34
4.1 Introduction ..... 34
4.2 Experimental data ..... 34
4.2.1 Test setups ..... 34
4.3 Comparison between the proposed method results and experimental data ..... 37
4.3.1 N-212-D1 ..... 38
4.3.2 N-216-D1 ..... 40
4.3.3 N-316-D1 ..... 42
4.3.4 N-212-D2 ..... 44
4.3.5 C-216-D1 ..... 46
4.3.6 C-216-D2 ..... 48
4.3.7 H-316-D1 ..... 50
4.3.8 B1 ..... 52
4.4 Discussion of results ..... 53
4.4.1 Discussing the FRP reinforced beams case ..... 53
4.4.2 Discussing steel reinforced beam case ..... 56
5 CONCLUSION ..... 57
REFERENCES ..... 60
APPENDIX ..... 64
Appendix A: User manual of using the working excel files ..... 65

# LIST OF TABLES

Table 3.1: Constitutive law for concrete under comprission ..... 20

Table 3.2: Constitutive law for concrete under tension ..... 21

Table 3.3: Secant modulus values for different stress levels and materials..... 28

Table 4.1: Geometrical properties of the studied beams ..... 36

Table 4.2: Material properties of the tested beams..... 37

Table 4.3: Ratios of applied methods under serviceability load - beam N-212-D1 .. 39

Table 4.4: Ratios of applied methods under higher load levels - beam N-212-D1 ... 39

Table 4.5: Ratios of applied methods under serviceability load - beam N-216-D1 .. 41

Table 4.6: Ratios of applied methods under higher load levels - beam N-216-D1 ... 41

Table 4.7: Ratios of applied methods under serviceability load - beam N-316-D1 .. 43

Table 4.8: Ratios of applied method under higher load levels - beam N-316-D1 .... 43

Table 4.9: Ratios of applied methods under serviceability load - beam N-212-D2 .. 45

Table 4.10: Ratios of applied methods under higher load levels - beam N-212-D2 . 45

Table 4.11: Ratios of applied methods under serviceability load - beam C-216-D1 47

Table 4.12: Ratios of applied methods under higher load levels - beam C-216-D1 . 47

Table 4.13: Ratios of applied methods under serviceability load - beam C-216-D2 49

Table 4.14: Ratios of applied methods under higher load levels - beam C-216-D2 . 49

Table 4.15: Ratios of applied methods under serviceability load - beam H-316-D1 51

Table 4.16: Ratios of applied methods under higher load levels - beam H-316-D1 . 51

Table 4.17: Ratios of applied methods under serviceability load - beam B1 ..... 53

Table 4.18: Ratios of applied methods under higher load levels - beam B1 ..... 53

Table 4.19: Comparing the ratios of the applied methods for serviceability loads of FRP reinforced beams..... 54

Table 4.20: Comparing the ratios of the applied methods for higher load levels of FRP reinforced beams ..... 55
Table 4.21: Comparing standard deviation of the applied methods for serviceability loads of FRP reinforced beams ..... 55
Table 4.22: Comparing the standard deviation of the applied methods for higher load of FRP reinforced beams levels..... 56

# LIST OF FIGURES

Figure 2.1: Moment/curvature relationship in beam ..... 5

Figure 2.2: Sections and layers for a typical beam..... 9

Figure 2.3: Conventional load - deflection behavior for a concrete member ..... 10

Figure 2.4: Experimental vs. calculated deflection using different approaches..... 16

Figure 3.1: Stress-Strain Relationship of Reinforcing Steel ..... 18

Figure 3.2: Stress-strain Relationship of FRP Reinforcing Bars..... 19

Figure 3.3: Hognestad's parabolic relationship ..... 19

Figure 3.4: Modified Bazant & Oh relationship..... 20

Figure 3.5: Cross section segments for finding I..... 23

Figure 3.6: Effective modulus of elasticity ..... 24

Figure 3.7: Layers for the effective "E" in case I ..... 26

Figure 3.8: Layers for the effective "E" in case II..... 27

Figure 3.9: M/EI diagram for the verification experimental work..... 29

Figure 3.10: Flow chart explaining the proposed method ..... 31

Figure 3.11: Four-point bending case ..... 32

Figure 4.1: Test setups and details (mm) ..... 35

Figure 4.2: Shows the test setups and details for steel beam ..... 36

Figure 4.3: Beam N-212-D1 results within serviceability loads ..... 38

Figure 4.4: Beam N-212-D1 results of full behavior..... 38

Figure 4.5: Beam N-216-D1 results within serviceability loads ..... 40

Figure 4.6: Beam N-216-D1 results of full behavior..... 40

Figure 4.7: Beam N-316-D1 results within serviceability loads ..... 42

Figure 4.8: Beam N-316-D1 results of full behavior..... 42

Figure 4.9: Beam N-212-D2 results within serviceability loads ..... 44
Figure 4.10: Beam N-212-D2 results full behavior ..... 44
Figure 4.11: Beam C-216-D1 results within serviceability loads ..... 46
Figure 4.12: Beam C-216-D1 results of full behavior ..... 46
Figure 4.13: Beam C-216-D2 results within serviceability loads ..... 48
Figure 4.14: Beam C-216-D2 results of full behavior ..... 48
Figure 4.15: Beam H-316-D1 results within serviceability loads ..... 50
Figure 4.16: Beam H-316-D1 results full behavior ..... 50
Figure 4.17: Beam B1 results within serviceability loads ..... 52
Figure 4.18: Beam B1 results full behavior ..... 52

# LIST OF SYMBOLS

## Greek Symbols:

$\beta_1$ coefficient has different values according to codes. It can be calculated from Equations (2.10), (3.14)

$\delta_{max}$ maximum deflection under applied moment

$\varepsilon_o$ characteristic strain in concrete under compression equals 2f'c/Ec

$\varepsilon_{cm}$ maximum applied compressive strain on concrete under the applied load

$\varepsilon_{cr}$ cracking strain of concrete

$\varepsilon_f$ strain in FRP reinforcement under the applied load

$\varepsilon_y$ yielding strain of steel reinforcement

$\zeta$ distributing coefficient, given by Equation (2.10)

$\eta$ coefficient equals to $[ 1 - (I_{cr}/I_g)]$

$\kappa_{cr}$ curvature at the section by ignoring concrete in tension

$\kappa_{uncr}$ curvature at the uncracked transformed section

$\rho$ reinforcement ratio

$\rho_{fb}$ balanced reinforcement ratio for FRP reinforced sections under bending

$\sigma_s$ tensile stress in reinforcement corresponding to applied load

$\sigma_{sr}$ tensile stress in reinforcement corresponding to first cracking (i.e. $M = M_{cr}$) which is calculated by ignoring tensile forces in concrete

$\Phi$ slope of elastic curve

$\Psi$ curvature

## Alphabetic Symbols:

**$A_M$** the area of the curvature diagram between the two points

**b** width of cross section

**c** depth of neutral axis

**c'** height of uncracked segment of concrete in tensile zone below the neutral axis

**d** effective depth of cross section

**d'** concrete cover

**$d_b$** diameter of the FRP reinforcement bars

**$E_c$, $E_o$** initial tangential modulus of elasticity of concrete

**$E_{eff}$** effective moment of inertia

**$E_f$** modulus of elasticity of FRP

**$E_s$** modulus of elasticity of steel in elastic region

**$E_{sc}$** secant modulus of elasticity of concrete under compression under applied stress level

**$E_{sh}$** modulus of elasticity of steel in strain-hardening region

**$E'_{st}$** secant modulus of elasticity in the middle of second layer below N.A

**$E''_{st}$** secant modulus of elasticity in the middle of third layer below N.A

**$E_{st}$** secant modulus of elasticity of concrete under tension under applied stress level

**EI** rigidity of cross section

**$f'_c$** concrete strength under compression corresponding to 28 days standard cylindrical specimen

**$f_{ct}$** concrete strength under tension

$\mathbf{f_f}$ fracture stress in steel

$\mathbf{f_{fu}}$ ultimate stress of FRP

$\mathbf{f_u}$ ultimate stress in steel

$\mathbf{f_y}$ yielding stress of steel reinforcement

**h** height of cross section

$\mathbf{I_{avg}}$ moment of inertia corresponding to average bending moment $M_{avg}$ under applied load

$\mathbf{I_{cr}}$ moment of inertia of the cracked transformed section

$\mathbf{I_e}$ equivalent moment of inertia

$\mathbf{I_g}$ moment of inertia of the gross section about the centroidal axis

$\mathbf{I_{min}}$ moment of inertia corresponding to maximum bending moment $M_{max}$ under applied load

$\mathbf{L_g}$ uncracked length of the beam in which $M<M_{cr}$

$\mathbf{M_a}$ maximum moment in the member under the applied load stage

**M, $\mathbf{M_b}$** bending moment

$\mathbf{M_{cr}}$ cracking moment

$\mathbf{M_u}$ ultimate moment that causes failure of member

**v(x)** deflection in terms of x

$\bar{x}$ Centroidal distance of the curvature between zero and x from the beam left end

**Y** height of the segment below neutral axis in cracked cross section, Y= d – c

# Chapter 1

# INTRODUCTION

## 1.1 Importance of research

Deflection control is one of the important design criteria. Codes suggest limits for deflection to provide reasonable comfort for the occupants of buildings, and to minimize the possibility of damage to finishing material. Thus the role of deflection control is essential in design. In the case of elastic materials, deflection can be calculated easily and accurately, but in the case of reinforced concrete, which has nonlinear behavior, the calculations become much more complicated. However, within the serviceability limits and prior to concrete cracking, the deflection can be estimated with good accuracy due to the linear behaviour of concrete. After cracking and under higher load levels, nonlinearity becomes more dominant and the estimation of deflection becomes more challenging.

By reviewing the literature it was discovered that there are many deflection formulas, some proposed by codes. However, most of these formulas have empirical nature or cannot predict deflection accurately over the entire loading range up to failure. This calls for improved and more accurate formula to calculate deflection.

## 1.2 Long term vs. short term deflection

The initial deflection occurs when loads are imposed on a beam and measure the corresponding deflection immediately. If other factors are considered in the calculations (e.g. complex effects of cracking, shrinkage, creep and construction loading), then long-term deflection can be calculated. In the long-term deflection, the deflection increases with increasing time for 5 to 10 years. However, the magnitude and rate depends on various factors including material, design, construction, and environmental factors. (Taylor, 1970)

## 1.3 Objective of the research

The objective of this research is to propose, implement and verify a refined method for calculating the short-term deflection of reinforced concrete beams, with special focus on FRP reinforced concrete members, which can be used to trace the full load-deflection response of beams subjected to monotonic loads. The study will be limited to short-term deflection and will only deal with statically determinant beams.

## 1.4 Introduction to chapters

This study is presented in five chapters as follows:

Chapter 1 gives a brief introduction to the thesis topic and describing the contents of each chapter.

In chapter 2, literature review about the deflection theory of flexural members and factors affecting tension stiffening are discussed. It also includes the historical overview of tension stiffening phenomenon and the proposed models to account for tension stiffening in the deflection calculations.

Chapter 3 discusses the proposed method. It starts by identifying the constitutive materials laws used in this research work, and then explains how to modify the components of the differential equation of deflection of flexural members. A step-by-step procedure for applying this method is presented.

Chapter 4 includes the verification of the proposed method, and compares its results with an experimental work and common code methods. The verification is based on seven FRP reinforced concrete beams which vary in reinforcement ratio, effective depth of the section, width of the section, and materials properties. It shows that the results of the proposed method are acceptable after comparison with experimental data better than the predictions of some common code methods.

In the last chapter, conclusions are drawn according to the literature review and the verification of the proposed method. Suggestion for practical implementations are made in this chapter.

# Chapter 2

# LITERATURE REVIEW

## 2.1 Introduction

This chapter presents an overview of deflection theory and the main concepts involved where the differential equation is formed and simplifications are made to arrive at formula for practical applications.

Moreover, main factors influencing deflection (creep, shrinkage, and tension stiffening) are examined, especially, detailed information about tension stiffening is given.

Historical overview about tension stiffening is given, fields of application and factors affecting tension stiffening are examined in details. Moreover, decaying of tension stiffening effect is discussed according to recent research findings. In addition, problems arising when tension stiffening in flexural members is ignored. However, tension stiffening concept can be clearly monitored in prestressed concrete as explained in this chapter. In addition to monotonic loading, effect of cyclic loading on deflection is briefly discussed later in this chapter. Furthermore, new concept in which tension stiffening occurs under tensile load is discussed. This concept is dubbed negative tension stiffening. Moreover, models of tension stiffening in widely used codes formula are highlighted. Finally, the effect of reinforcement ratio on tension stiffening is explained with graphs along with comparison between ACI and Eurocode

methods and the experimental results. Also, the effect of neglecting its effect is investigated by comparing the predicted deflection values with and without tension stiffening with corresponding experimental data.

## 2.2 Deflection theory

By the advancement of science and creativity of architects the demand for open areas where concrete members must span large distances is becoming common occurrence. This has encouraged architects to span even larger distances without intermediate supports, but for structural engineers it has created the problem of deflection control.

Figure 2.1 shows a typical segment of the deflection curve in a member due to bending, which shows its vertical deflection v(x) at distance x from the left end in the beam and its slope Φ at the same location:

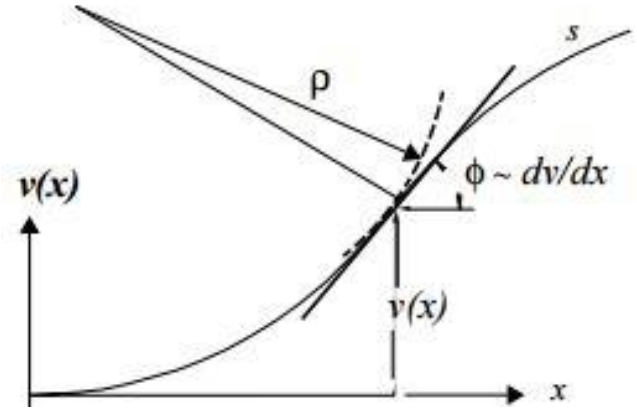


Figure 2.1: Moment/curvature relationship in beam

From basic mechanics (Popove, 1998) the differential equation in the case of pure bending can be written as:

$$\frac{M_b}{E\,I} = \frac{d\varphi}{ds} \tag{2.1}$$

where: s is the centroidal axial coordinate of any point along the beam measured from its left end, $M_b$ is the bending moment acting on the beam, and EI its flexural rigidity.

However, curvature of the member need to be related to its transverse displacements. This can be done by direct application of classical calculus resulting in:

$$\Psi = \frac{d\varphi}{ds} = \frac{\frac{d^2v}{dx^2}}{\left\{1 + \left(\frac{dv}{dx}\right)^2\right\}^{\frac{3}{2}}} = \frac{V''}{\{1 + (V')^2\}^{\frac{3}{2}}} \tag{2.2}$$

where $v'$ and $v''$ are the first and second derivative of deflection with respect to x.

So whenever bending moment is given in terms of x, this non-linear, second order, ordinary differential equation can be solved to obtain the transverse displacement (deflection) in terms of x. However, solving this kind of differential equation is not an easy thing but Leonhard Euler manipulated and solved this equation back in eighteenth century for extremely complex end-loading conditions. However, going into that much details can be avoided by the usual assumption of having small rotations and displacement where $\left(\frac{dv}{dx}\right)^2 < 1$. This implies that slope of the deflected beam is small with respect to 1 or in another words the rotation of the cross section is less than 1 radian, which results in:

$$\Psi = \frac{d^2v}{dx^2} = \frac{M_b(x)}{E\,I} \tag{2.3}$$

Equation (2.3) may be integrated twice to obtain the beam deflection equation as:

$$v(x) = \int_0^x dx \int_0^x \psi dx \tag{2.4}$$

Equation (2.4) represents the well-known double integration formula deflection. In the case of linear elastic and homogeneous beams, the curvature $\psi$ in Equation (2.4) can be replaced by $\frac{M}{EI}$ per Equation (2.3), in which case Equation 4 becomes:

$$v(x) = \int_0^x dx \int_0^x \frac{M}{EI} dx \tag{2.5}$$

In Equation (2.5) the second integral represents the area of the curvature diagram from zero to a distance x while the first integral represents the distance from beam end to the centroid of the curvature diagram. Therefore it may be written as:

$$v(x) = \int_0^x x \frac{M}{EI} dx = \bar{x} A_M \tag{2.6}$$

where $\bar{x}$ is the centroidal distance of the curvature diagram between zero and x from the beam left end and $A_M$ is the area of the curvature diagram between the two points. Equation (2.6) is the well-known mathematical representation of the so-called **second moment-area theorem.** This theorem will be used later on to calculate the deflection of reinforced concrete beams over the complete loading range, involving linear or nonlinear material behavior.

When this simplified formula is considered for elastic materials, it yields quite accurate results but as non-linear behavior starts to appear, the results of this formula deviate from the accepted values. Therefore, modifications to this formula are needed to account for material and/or geometric non-linearity.

## 2.3 Extension of elastic deflection theory to inelastic non homogeneous beams

The above relationships can be extended to beams comprising sections undergoing linear or nonlinear deformations under the assumption of small deflection theory. In this case, one can either express the curvature of the beam directly as function of its material properties at each section or alternatively compute the flexural rigidity of the section at each section based on the constitutive laws of the material comprising the cross-section. The quantity E in the case of nonlinear materials represents the tangential or secant modulus rather than the elastic modulus. Hence, to trace the load-deflection response, one must perform a series of analyses by gradually increasing the applied load in small increments and then compute the EI value for each load increment. Hence in this case, increments of deflection $\Delta v$ can be computed for increments of moment $\Delta M$ using:

$$\Delta v = \sum_{i=1}^{n} \bar{x}_i \frac{\Delta M_i}{\sum_{j=1}^{m} \frac{1}{3} E_{ij} b_{ij} (z_j^3 - z_{j-1}^3)} \tag{2.7}$$

In Equation (2.7), m represents the number of layers that each cross-section i is divided in, n represents the number of cross-sections considered between points $x_1$ and $x_2$ along the beam, $E_{ij}$ and $b_{ij}$ represent the tangent modulus and width of the layer ij and $z_j$ and $z_{j-1}$ represent the distance of the bottom and top of layer j from the neutral axis, respectively. Notice that positive z points upward. Figure 2.2 illustrates the sections and layers for a typical beam.

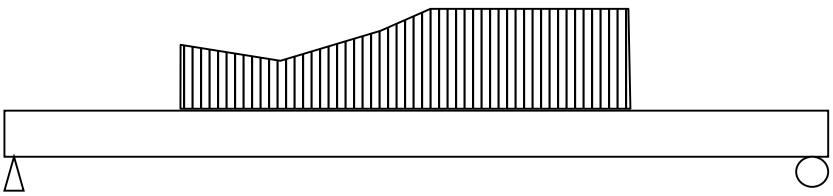

(a) Beam

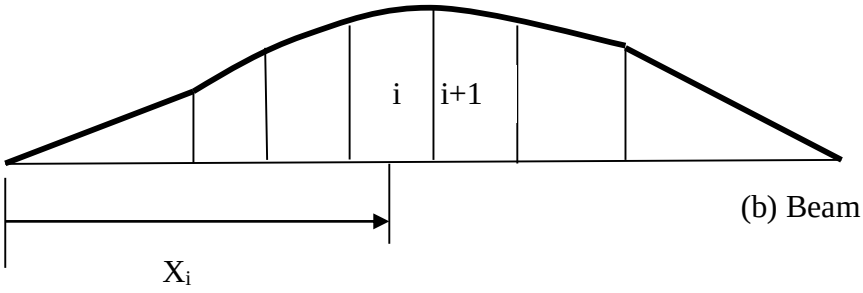


(b) Beam Bending Moment Diagram

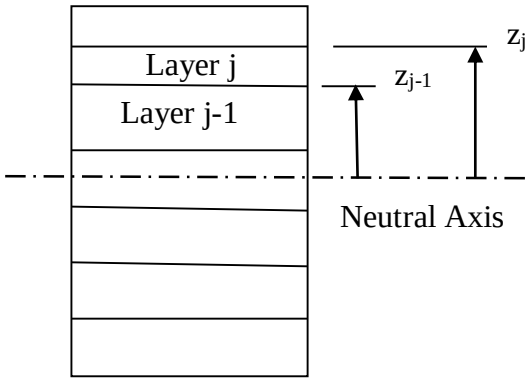


(c) Beam Cross Section and its Division into Layers

Figure 2.2: Sections and layers for a typical beam, (a) Beam , (b) Beam bending moment diagram, (c) Beam cross section and its division into layers

Equation (2.7) is general and applies to any cross-section or material composition acting linearly or nonlinearly. A layer can be made of any material provided it is fully bonded to its adjacent layers and acts fully compositely.

However, in this study, a simplified version of the procedure explained before is applied.

It should be kept in mind the importance of other factors related to the concrete itself such as: material properties, loading level, and time, which affect the long-term deflection behavior in general. These factors are: creep, shrinkage, and tension stiffening of reinforced concrete. As this research is interested in short-term deflection

of reinforced concrete beams, the concept of tension stiffening will be discussed in more detail.

### 2.3.1 Tension stiffening

Tension stiffening is the ability of the uncracked concrete between two cracks to carry tensile stresses in reinforced concrete. Figure 2.3 illustrates the effect of tension stiffening on the deflection of a concrete member.

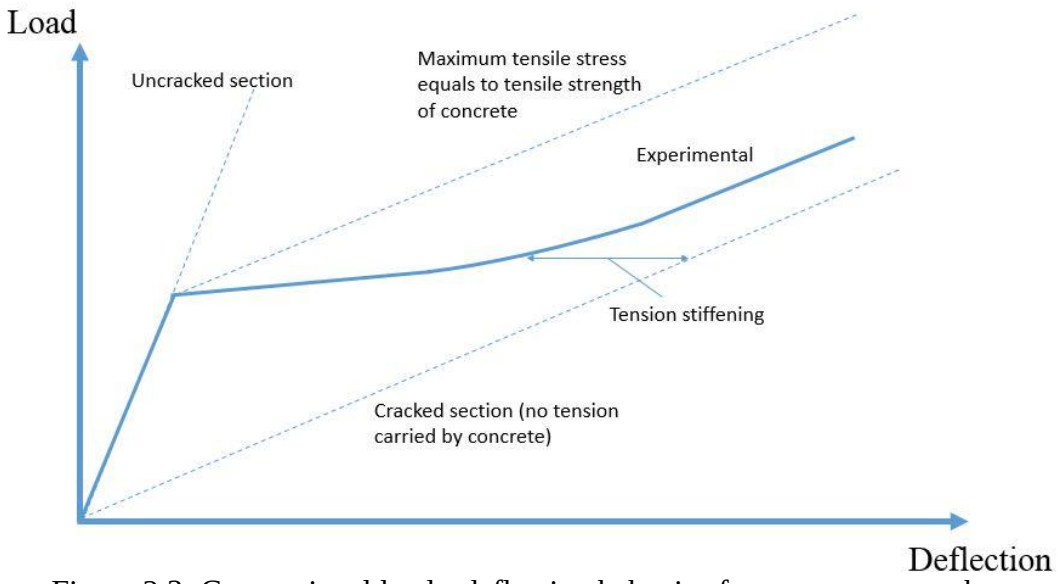


Figure 2.3: Conventional load - deflection behavior for a concrete member

#### 2.3.1.1 Historical overview

The contribution of tension-stiffening was neglected in the early days of concrete technology due to its minor effect on the concrete ultimate strength. It remained neglected up to the 70s, but subsequently was introduced in the analysis of deflection characteristics of reinforced concrete, and in 80s it appeared in the design codes recommendations. (Stramandinoli & La Rovere, 2008)

Obviously the concrete at cracked section has no tension strength but the concrete between two cracks can carry tension. This contribution to tensile resistance gradually

decreases as the tensile stress (strain) in the embedded tensile reinforcement increases. Thus tension stiffening reduces the deformation of the reinforcement, resulting in less curvature, and leads to reduced level of deflection of the reinforced member. In other words, it gives extra stiffness to the member and is thus called tension stiffening.

#### 2.3.1.2 Fields of application

From this point it can be realized that the effect of tension stiffening of reinforced concrete is essential for the assessment of the performance of reinforced concrete structures. It is also widely used in a variety of fields of knowledge in reinforced concrete. For instance: as mentioned earlier, the deflection of flexural members might be one of the most important applications of this principle. However, it has more effect on the lightly reinforced members (slabs) than the heavier reinforced ones (beams) which will be discussed in details later (Gilbert, 2007). Another issue that concerns with tension stiffening is the ductility of reinforced members where structural engineers consider the ductility of reinforced structures as an important characteristic. However, this is directly related to the bond characteristics ($M_u$, reinforcement) as it affects the rigid body rotation of the plastic hinges of reinforced members in which tension stiffening has a significant impact on this behavior (Haskett, Oehlers, Ali, & Wu, 2009). Crack propagation is also affected by the behavior of the reinforced concrete. Moreover, the performance based design and its applications are based on the deflection calculations which are affected by tension stiffening.

#### 2.3.1.3 Factors affecting tension stiffening

There are many factors affecting this phenomenon, including the dimensions of the member, and the reinforcement characteristics (material, condition, ratio, number of bars and their diameter/s, modular ratio …etc.).

#### 2.3.1.4 Tension stiffening decaying

However, tension stiffening is time dependent and it has a high short-term effect which drops to a lower long-term one within 20 days. However, in real life practice the long-term behavior is more important than the short-term one. The effect of tension-stiffening reduces to approximately half of its short-term effect. Moreover, the specimens with higher reinforcement ratios show shorter decay times while lightly reinforced slabs show longer time. (Scott & Beeby, 2005)

It should be kept in mind that the increase in concrete member deflection is due to three main reasons: creep, shrinkage, and the loss of tension stiffening in which all of these factors are time dependent.

#### 2.3.1.5 Tension stiffening in flexural members

Unfortunately, the study of tension stiffening effect on flexural members is problematic because the strain in flexural members can be measured relatively accurate but the stresses which initiate these strains cannot be measured. In addition, in the long term, the effects of creep on the compression zone and shrinkage influence the tension stiffening effect. That is the reason why the majority of researchers have concentrated their experimental works on members subjected to pure tension.(Scott & Beeby, 2005)

#### 2.3.1.6 Tension stiffening in prestressed concrete

Although many researchers worked on the tension stiffening of reinforced concrete, less attention has been paid to this phenomenon in prestressed concrete. Even those who conducted research on the prestressed concrete did it under direct tension, not flexural, and concluded that the prestressing forces enhanced the tension stiffening behavior. However, the contribution of tension stiffening in fully prestressed concrete

sections are found to be negligible from the practical way of view. (Gar, Head, & Hurlebaus, 2012)

#### 2.3.1.7 Cyclic loading

The deformation behavior of reinforced concrete structures are intensively related to the unloading and reloading (UR) cycles in which it affects the tension stiffening behavior. A typical example of this problem arises in flat concrete slabs due to punching shear resistance in which it depends on the slab rotation. In this particular case the slab had to be unloaded and post-installed strengthening was required. This is the case in a variety of structural strengthening techniques. (Koppitz, Kenel, & Keller, 2014)

#### 2.3.1.8 Negative tension stiffening

Some researchers observed an increase in the stiffness of the concrete between cracks while unloading. That is the case when the concrete in tension zone starts to take compression stresses and prevent the reinforcement from retrieving to its original state. This is called negative tension stiffening effect which was experimentally observed by Gómez Navarro and Lebet (Zanuy, de la Fuente, & Albajar, 2010).

#### 2.3.1.9 Models considering tension stiffening

Many models have been proposed to account for the tension-stiffening in the deflection calculations ranging from simple to complex. One of the simplest models rely on considering an equivalent moment of inertia for the cracked beam section which is proposed by Branson in 1968– which is used method to calculate deflection in ACI-318-2005.

$$I_e = \left(\frac{M_{cr}}{M_a}\right)^3 I_g + \left[1 - \left(\frac{M_{cr}}{M_a}\right)^3\right] I_{cr} \leq I_g \qquad (2.8)$$

where: $I_{cr}$ = moment of inertia of the cracked transformed section, $I_g$ = moment of inertia of the gross section about the centroidal axis, $M_a$ = maximum moment in the member under the applied load stage, and $M_{cr}$ = cracking moment.

Other researchers have examined the effect of tension stiffening on continuous composite beams and end up with simplified method by modifying the cross sectional area (Fabbrocino, Manfredi, & Cosenza, 2000), some other models modifies the sectional area including ACI-440 (ACI Committee 2005) and Behfarnia (2009).

Other models modify the constitutive laws of concrete or reinforcement (Steel, FRPs…etc.) after cracking. However, these models were mainly proposed for nonlinear finite element analysis. Some models which modify the steel constitutive equation are: Gilbert and Warner (1978), Choi and Cheung (1996) and the CEB manual design model (1985). Among those which modify the concrete constitutive law are: Scanlon and Murray (1974), Lin and Scordelis (1975), Collins and Vecchio (1986), Stevens et al. (1987), Balakrishnan and Murray (1988), Massicotteet al., Renata et al (1990). (Stramandinoli & La Rovere, 2008)

The most complex models rely on the bond stress – slip mechanism. Among those who worked on these models: Marti et al. (1998), Floegl and Mang (1982), Gupta and Maestrini (1990), Wu et al. (1991), Russo and Romano (1992), Choi and Cheung (1996), and Kwak and Song (2002). (Stramandinoli & La Rovere, 2008)

It is worth mentioning that the current approach applied in Eurocode 2 (1994) which involves the calculation of curvature at specific cross section followed by integrating it to obtain the deflection.

$$\kappa = \zeta \kappa_{cr} + ( 1 - \zeta ) \kappa_{uncr} \quad (2.9)$$

where: $\kappa_{cr}$ = curvature at the section by ignoring concrete in tension, $\kappa_{uncr}$ = curvature at the uncracked transformed section, and $\zeta$ = distributing coefficient stands for degree of cracking and moment level and is given as:

$$\zeta = 1 - \beta_1 \beta_2 \left( \frac{\sigma_{sr}}{\sigma_s} \right)^2 \quad (2.10)$$

where: $\beta_1$ = 0.5 for plain bars and 1.0 for deformed one; $\beta_2$ = 1.0 for single, short-run load and 0.5 for repeated or sustained loading; $\sigma_{sr}$ = tensile stress in reinforcement corresponding to first cracking (i.e. M = $M_{cr}$) which is calculated by ignoring tensile forces in concrete; $\sigma_s$ = tensile stress in reinforcement corresponding to applied load.

#### 2.3.1.10 Tension stiffening relationship with reinforcement ratio

It has been mentioned before that amount of reinforcement provided in the concrete members has key role in the tension stiffening contribution to deflection (Gilbert, 2007). This can be best demonstrated by a comparison between the deflections of concrete slab with varied amount of reinforced ($\rho$) in which the same concrete properties and loading level is maintained for all of the specimen. The results are illustrated in Figure 2.4.

It is obvious that the difference between experimental results and theoritical ones excluding tension stiffening has discending trend as the reinforcement ratio increases. Moreover, by closely examining this graph it can be realized that the Eurocode method results in better estimations rather than ACI method at any reinforcement ratio whereas ACI results improves as the reinforcement ratio increases This demonstrates the effectiveness of using the above curvature method to calculate the deflection of reinforced concrete members.

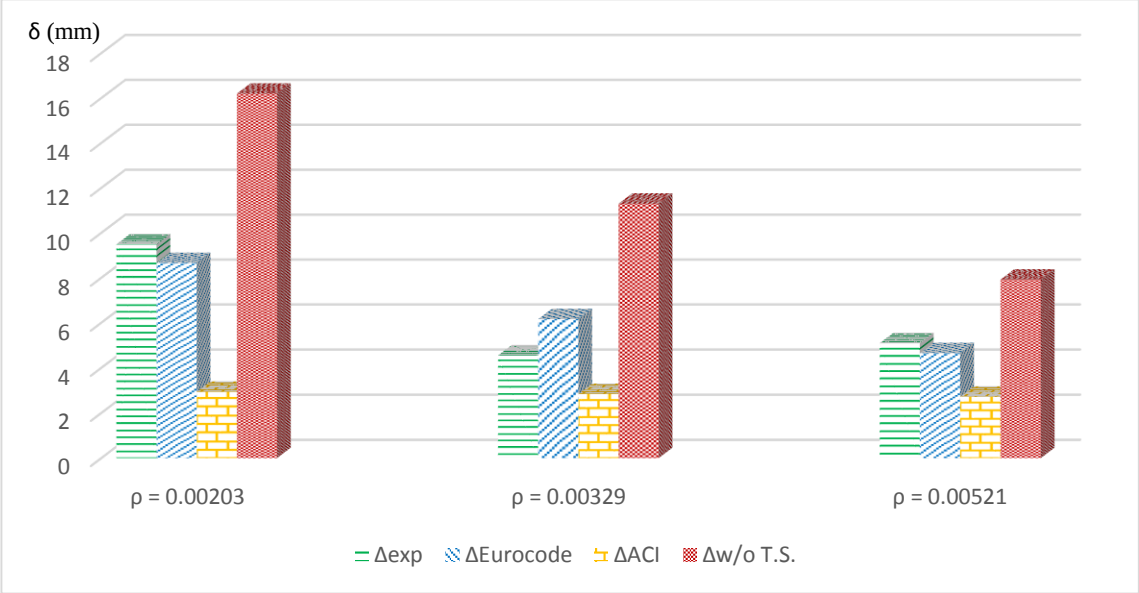


Figure 2.4: Experimental vs. calculated deflection using different approaches (Gilbert, 2007)

# Chapter 3

# PROPOSED METHOD

## 3.1 Introduction

This chapter includes the method used in this research. This method consists of several steps. It involves modifications of moment of inertia of the section and strain-dependent elastic modulus values as well as application of the tension-stiffening concept in calculations. First of all the concrete and reinforcement constitutive laws used in this method are presented. Then the procedure used to solve the differential equation of deflection (i.e. Moment-area method) in conjunction with the appropriate constitutive laws and tension stiffening model are explained. The proposed concept for calculating the moment of inertia is explained and the required details are given in order to facilitate calculations. Then modifications of modulus of elasticity are introduced using the concept of effective modulus of elasticity and secant elastic modulus. Later on a step-by-step procedure for calculating the deflection is explained and a flow chart demonstrating the process is introduced.

## 3.2 Constitutive laws of reinforced concrete

The value of $E_{ij}$ for any layer is function of the stress-strain relationship of its constituent material. For materials which have different stress-strain relationship in tension versus compression, the appropriate constitutive law must be used. For example, concrete and FRP have different constitutive laws in tension versus compression. Therefore, in this study the constitutive laws used will be described.

### 3.2.1 Steel reinforcement

Typical reinforcing steel in tension with minimum guaranteed yield stress of 400 MPa is modeled as an elasto-plastic strain hardening material as illustrated in Figure 3.1.

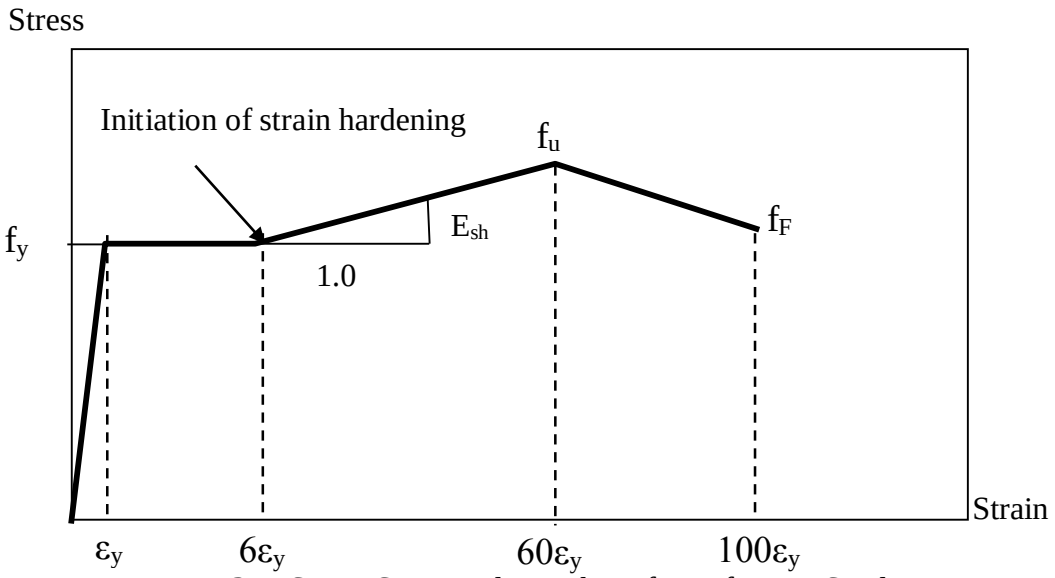


Figure 3.1: Stress-Strain Relationship of Reinforcing Steel

The slope of this curve at any stress or strain level represents the tangent modulus of this material.

In most properly reinforced beams, failure occurs before strain hardening of the steel while in slabs failure may occur after strain hardening, however, the bar strain practically never reaches the descending branch under monotonic loading of reinforced concrete members. Hence, practically, only the part up to $f_u$ is of interest.

### 3.2.2 Fiber reinforced polymer (FRP) reinforcement

FRP bars and grids are principally used as tensile reinforcement while their compressive strength is neglected in reinforced concrete members. In tension, FRP behaves as a linear elastic material up to failure as illustrated in Figure 3.2.

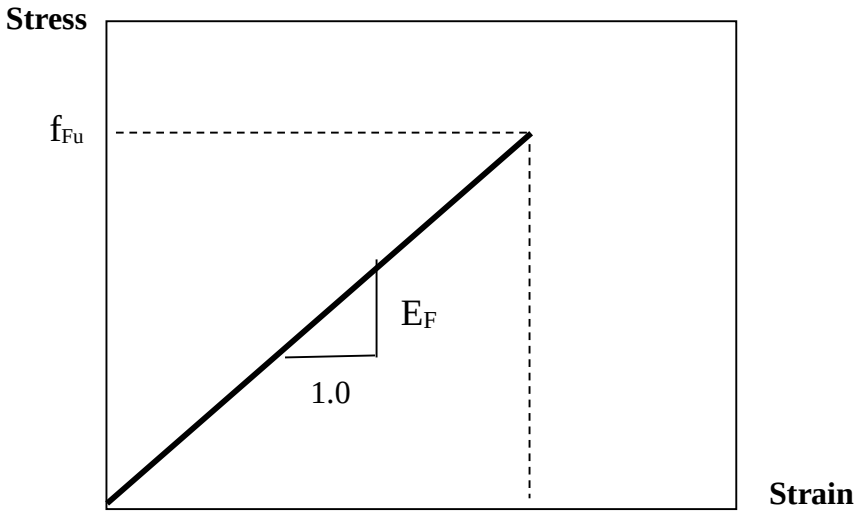

Figure 3.2: Stress-strain Relationship of FRP Reinforcing Bars

### 3.2.3 Concrete

#### 3.2.3.1 Concrete in compression

There are many constitutive laws idealizing the stress-strain behavior of concrete. However, the most common one is Hognestad's parabolic relationship as shown in Figure 3.3:

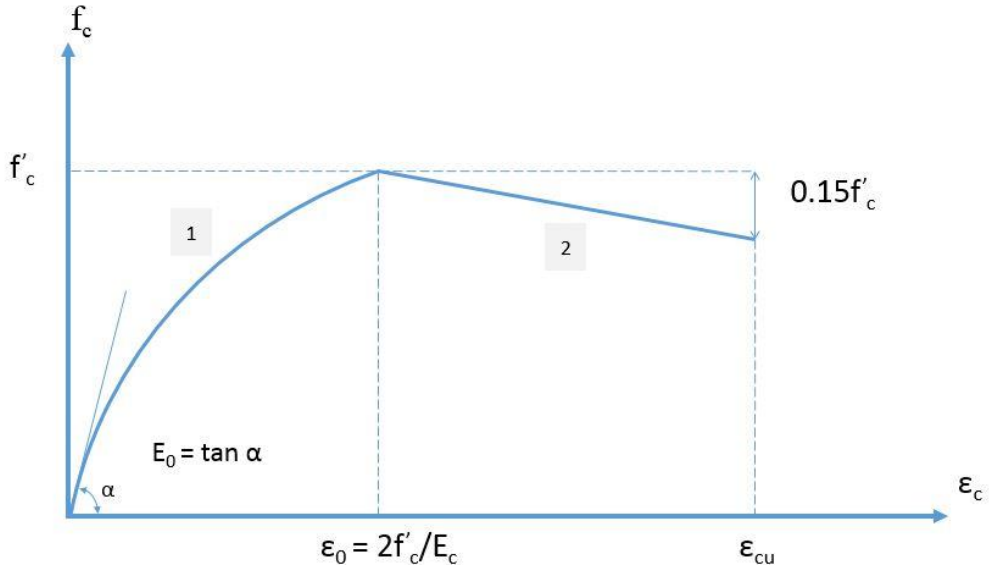

Figure 3.3: Hognestad's parabolic relationship (Park & Paulay, 1975)

The equations for this model are presented in Table 3.1:

Table 3.1: Constitutive law for concrete under compression

| | | |
|---|---|---|
| 1 | $\varepsilon_c \leq \varepsilon_0$ | $f_c = f'_c \left[\frac{2\varepsilon_c}{\varepsilon_o} - \left(\frac{\varepsilon_c}{\varepsilon_o}\right)^2\right]$ |
| 2 | $\varepsilon_c \geq \varepsilon_0$ | $f_c = f'_c\,[1 - 100(\varepsilon_c - \varepsilon_o)]$ |

N.B. f'c is based on standard cylindrical specimen. In the case of cubic samples, 0.85f'c is used instead of f'c.

### 3.2.3.2 Concrete in tension

Many idealization of the tensile stress-strain relationship of concrete under tension have been proposed by researchers. . However, the model which is used in this study is the Modified Bazant & Oh model (Bažant & Cedolin, 1991) as illustrated in Figure 3.4:

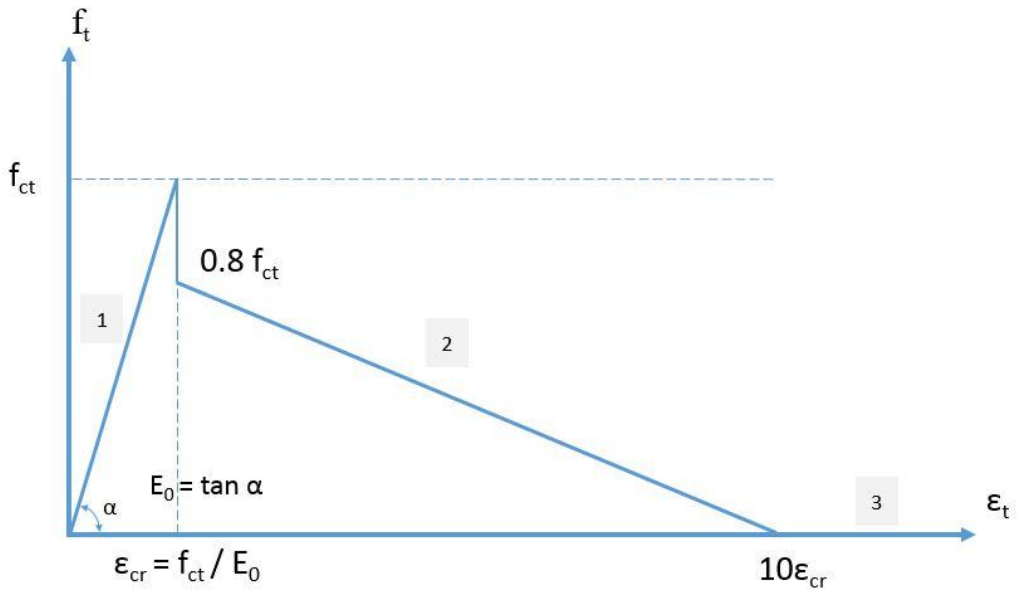


Figure 3.4: Modified Bazant & Oh relationship (Bažant & Cedolin, 1991)

The modification is taking the ultimate tensile strain to be $10\varepsilon_{cr}$ that is recommended by Prof. Dr. Razaqpur (personal communication) based on to his experience in this field. Thus, the constitutive law can be shown in Table 3.2 as follows:

Table 3.2: Constitutive law for concrete under tension

| | | |
|---|---|---|
| 1 | $\varepsilon_t \leq \varepsilon_{cr}$ | $f_t = E_o \varepsilon_t$ |
| 2 | $\varepsilon_{cr} \leq \varepsilon_t \leq 10\ \varepsilon_{cr}$ | $f_t = \frac{-0.8\ f_{ct}}{9\ \varepsilon_{cr}}\ \varepsilon_t + \frac{10}{9}\ 0.8\ f_{ct}$ |
| 3 | $\varepsilon_t > 10\ \varepsilon_{cr}$ | $f_t = 0$ |

## 3.3 Moment-area method

The purpose of this research since the rigidity of the beam will vary, depending on the region of the beam and its loading.

For simply supported prismatic and symmetrically loaded beams to calculate the maximum deflection, calculate the area below the M/EI diagram between the nearest support and the point of maximum deflection and multiply this area by the distance between its centroid and the nearest support In this case, the area below M/EI diagram can be divided into several segments especially if the moment of inertia varies along the beam varies significantly. For more general load and boundary conditions, this method can be applied with appropriate modifications as described in Popove and Balan (Popove, 1998).

To apply this method, the span of the beam is divided into several segments, with each segment having different E and I values. The way to calculate these values is

mentioned later in this chapter. Then by applying the moment-area method one can determine the deflection of the beam. As a general guide in dividing the beam, the first segment is the uncracked segment in which $M < M_{cr}$. Another segment is generally at the section where M reaches $M_{max}$. The segment between these two segments can be considered as the third segment. This is a simplification of this method, for hand calculation purposes, but considering more segments might lead to more accurate results but it requires the use of computers.

## 3.4 Moment of inertia

The moment of inertia is calculated using the concept of tension stiffening. So to include this effect neither $I_{gross}$ nor $I_{cr}$ are going to be used. Other methods like ACI and Eurocode use formula to find the appropriate I of the section under a specific applied moment profile. However, in this research an alternative method is proposed in order to calculate the deflection relatively accurately and expediently. One of the fundamental shortcomings of existing code-based formulas is that they assume the elastic modulus of concrete to be constant and independent of the level of strain in the concrete. In fact, the elastic modulus decreases with the level of strain, particularly when the concrete strain exceeds approximately 0.1% in compression.

Based on the equilibrium of the tension and compression forces in the cross-section, the depth of the neutral axis (c) can be calculated by iteration method. However, the calculation of this depth should include the contribution of the concrete in tension which has considerable capacity and it affects this equilibrium. Based on the maximum applied compressive strain on concrete under the given load state ($\varepsilon_{cm}$) and the depth of neutral axis (c) one can calculate all the relevant variables which are going to be used in calculating the moment of inertia.

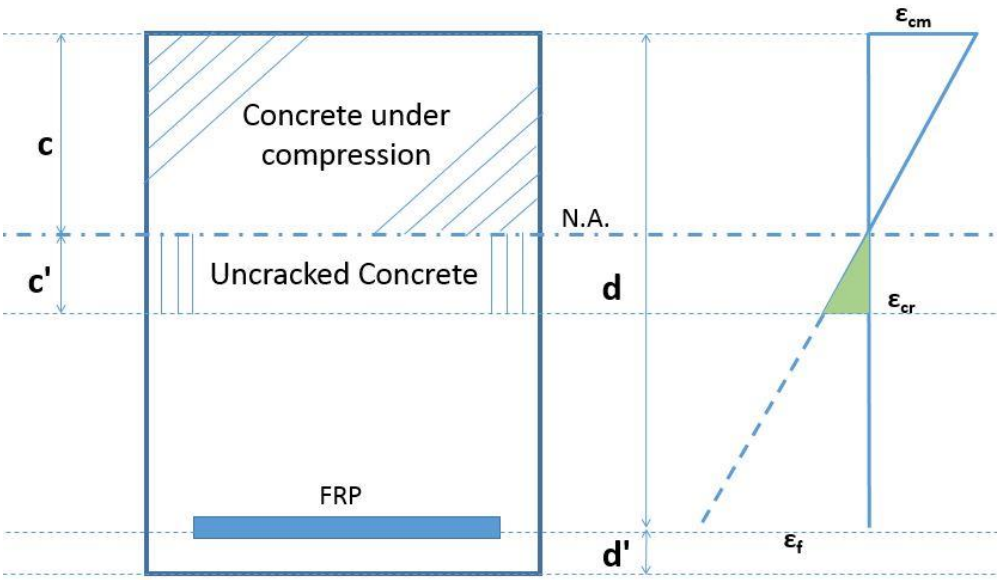

Figure 3.5: Cross section segments for finding I

From Figure 3.5 height of uncracked segment of concrete in tensile zone below the neutral axis (i.e. c') can be determined. Using similar triangles c' can be calculated from Equation (3.1) as follows:

$$c' = \frac{\varepsilon_{cr}}{\varepsilon_{cm}}\ c \tag{3.1}$$

Consequently one can calculate the moment of inertia under an applied moment based on moment of inertia concept as expressed in Equation (3.2):

$$I = \frac{b\,c^3}{12} + b\,c\,\left(\frac{c}{2}\right)^2 + \frac{b\,c'^3}{12} + b\,c'\,\left(\frac{c'}{2}\right)^2 + n\,A_f\,(h - c - d')^2 \tag{11}$$

## 3.5 Effective elastic modulus

As stated earlier, most of the well-known deflection methods assume the elastic modulus of the section to be constant and equal to the secant modulus of concrete ($E_o$), corresponding to stress of 0.4fc'. This assumption is reasonable, provided the maximum stress in the concrete does not exceed 0.4fc' or the approximate elastic limit of concrete. At the serviceability limit state, the assumption is generally reasonable.

However, at higher load levels, this is assumption is not correct and the actual elastic modulus may be significantly less than this value. It will depend on the level of stress or more accurate maximum strain in the concrete. On the other hand, the presence of FRP reinforcement also affects the elastic modulus of the section. Of course, the concept of transformed section, with proper values of elastic modulus for each concrete layer can easily account for the presence of any reinforcement.

Kwok et al. have proposed a method to include these effects together and called the equivalent elastic modulus the effective elastic modulus. (Aron Michael and Chee Yee, 2006)

Using that concept the cross section can be divided into layers as shown in Figure 3.6,

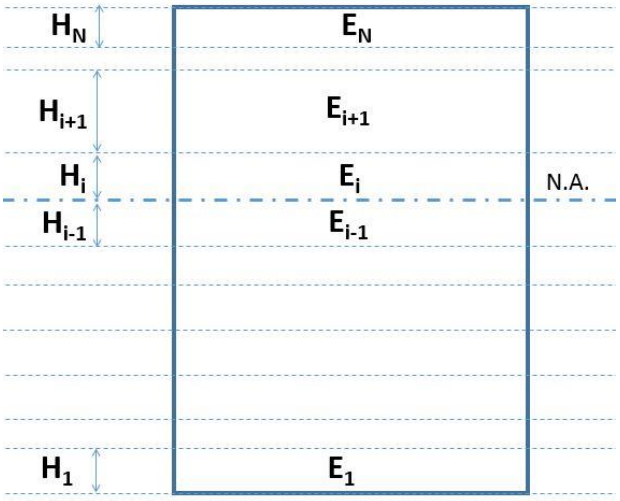

Figure 3.6: Effective modulus of elasticity

According to Kwok et al., the effective modulus of elasticity can be calculated using Equation (3.3) as follows:

$$E_{eff} = \frac{\sum_{i=1}^{N} H_i E_i}{\sum_{i=1}^{N} H_i} \quad (3.3)$$

In which: $H_i$ is the height of the $i^{th}$ layer, and $E_i$ is the average modulus of elasticity of the $i^{th}$ layer. This is clearly an approximation as it assumes the effective elastic modulus to be the weighted average of the elastic moduli of the various layers in a section. Still, it is much better than the assumption of a constant elastic modulus for the entire section or beam.

The number of layers to be used depends mainly on the stress level; particularly, the stress level on the tension side of the section. According to this concept, cases that arise in the tension part is discussed in the following sub-sections.

### 3.5.1 Classification of cases due to the stress level in tension part of cross section

Two unique cases can be faced. One of them is when all the tension part below the neutral axis is contributing to the tensile capacity of the section (i.e. 10 c' > Y = d – c). And the second case is when a portion of the tension part below the neutral axis provides tension stiffening to the section (i.e. 10 c' < Y= d – c).

#### 3.5.1.1 Case I: 10c' > Y= d – c and c' < Y = d – c

For the sake of simplicity, d will be used instead of h in this thesis. In this case, the cross section can be divided into the following layers as shown in Figure 3.7:

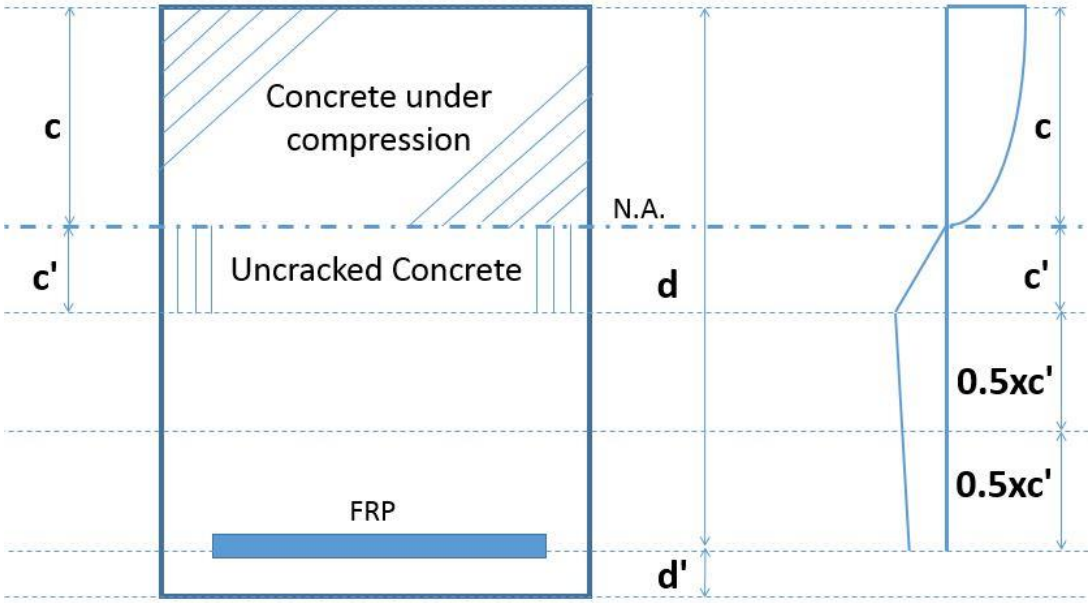

Figure 3.7: Layers for the effective "E" in case I

Then the secant elastic modulus in the middle of each layer is needed to be found and Equation (3.4) is applied:

$$E_{eff} = \frac{c\,E_{sc} + c'E_o + 0.5x\,c'E'_{st} + 0.5x\,c'\,E''_{st} + d_b\,E_f}{c + c' + xc' + d_b} \qquad (3.4)$$

where $E'_{st}$ is the secant modulus in the middle of second layer below N.A., and $E''_{st}$ is the secant modulus in the middle of third layer below N.A.

However, the value of x can be found by applying simple triangle similarity. And $d_b$ is the diameter of the FRP reinforcement bars used.

**3.5.1.2 Case II: 10 c' < Y = d – c**

In this case, the layers of the cross section can be determined as demonstrated in Figure 3.8:

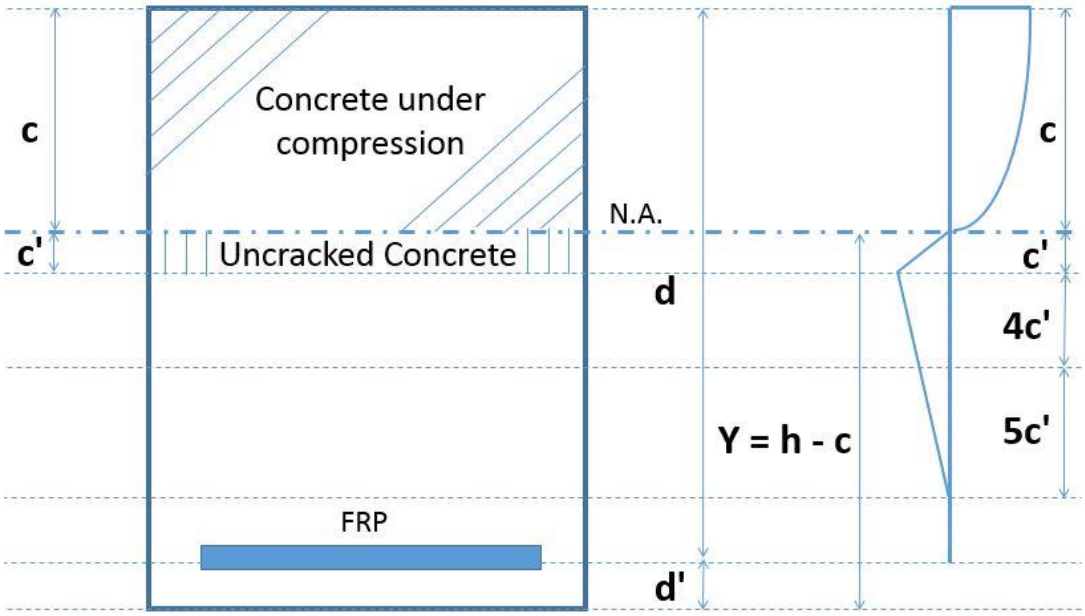

Figure 3.8: Layers for the effective "E" in case II

And by formulating this Equation (3.5) can be written to calculate the effective modulus of elasticity:

$$E_{eff} = \frac{c\,E_{sc} + c'\,E_{st} + 4c'\,E'_{st} + 5c'\,E''_{st} + d_b\,E_f}{c + c' + 4c' + 5c' + d_b} \quad (3.5)$$

where $E'_{st}$ is the secant modulus in the middle of second layer below N.A., and $E''_{st}$ is the secant modulus in the middle of third layer below N.A.

**3.5.1.3 Secant modulus of elasticity**

It is extremely important to use the secant modulus of elasticity for the equations mentioned above. The secant modulus can be obtained based on the constitutive laws described in the beginning of this chapter. For easy reference, the secant modulus of elasticity for the related constitutive laws can be obtained from Table 3.3 which provides the summary of the constitutive laws presented earlier.

Table 3.3: Secant modulus values for different stress levels and materials

| **Secant modulus = (Stress) / (corresponding strain)** | | |
|---|---|---|
| **Concrete under compression** | | |
| 1 | $\varepsilon_c \leq \varepsilon_0$ | $f_c = f'_c \left[\frac{2\varepsilon_c}{\varepsilon_o} - \left(\frac{\varepsilon_c}{\varepsilon_o}\right)^2\right]$ |
| 2 | $\varepsilon_c \geq \varepsilon_0$ | $f_c = f'_c [1 - 100(\varepsilon_c - \varepsilon_o)]$ |
| **Concrete under tension** | | |
| 1 | $\varepsilon_t \leq \varepsilon_{cr}$ | $f_t = E_o \varepsilon_t$ |
| 2 | $\varepsilon_{cr} \leq \varepsilon_t \leq 10\ \varepsilon_{cr}$ | $f_t = \frac{-0.8 f_{ct}}{9\ \varepsilon_{cr}} \varepsilon t + \frac{8}{9} f_{ct}$ |
| 3 | $\varepsilon_t > 10\ \varepsilon_{cr}$ | $f_t = 0$ |
| **FRP reinforcement** | | |
| 1 | $\varepsilon_f \leq \varepsilon_{cu}$ | $f_f = E_f \varepsilon_f$ |

## 3.6 Step-by-step procedure for calculating beam deflection

Using all the concepts mentioned earlier, the calculation steps are as follows:

(1) Find $M_{cr}$, $I_{cr}$, and $I_g$.

(2) Draw the bending moment diagram for applied load.

(3) Using the cross sectional analysis by equating the tensile and compression forces determine the depth of neutral axis (c), and the concrete compression strain in the extreme fiber ($\varepsilon_{cm}$). This process requires iterations, and this step should be repeated for two cross sections (at $M_{max}$, and $M_{avg}$; $M_{avg} = 0.5(M_{max} + M_{cr})$

(4) Calculate $E_{eff}$ for the extreme case (i.e. $M_{max}$) under the applied load as mentioned in (3.5)

(5) Calculate the moment of inertia corresponding to (c) and including the uncracked depth of the concrete (c'). "I" should be calculated twice under each load level (i.e. $I_{min}$ for $M_{max}$, and $I_{avg}$ for $M_{avg}$). Using Equation (3.2).

(6) Find the deflection of the beam under the applied loads using the **second moment-area theorem.**

For the case of four-points bending load, which is the case of verification, If $M_{max} < M_{cr}$ then the elastic deflection method can be used. Otherwise if $M_{max} > M_{cr}$, the M/EI diagram is shown in the Figure 3.9 and the deflection formula is given as:

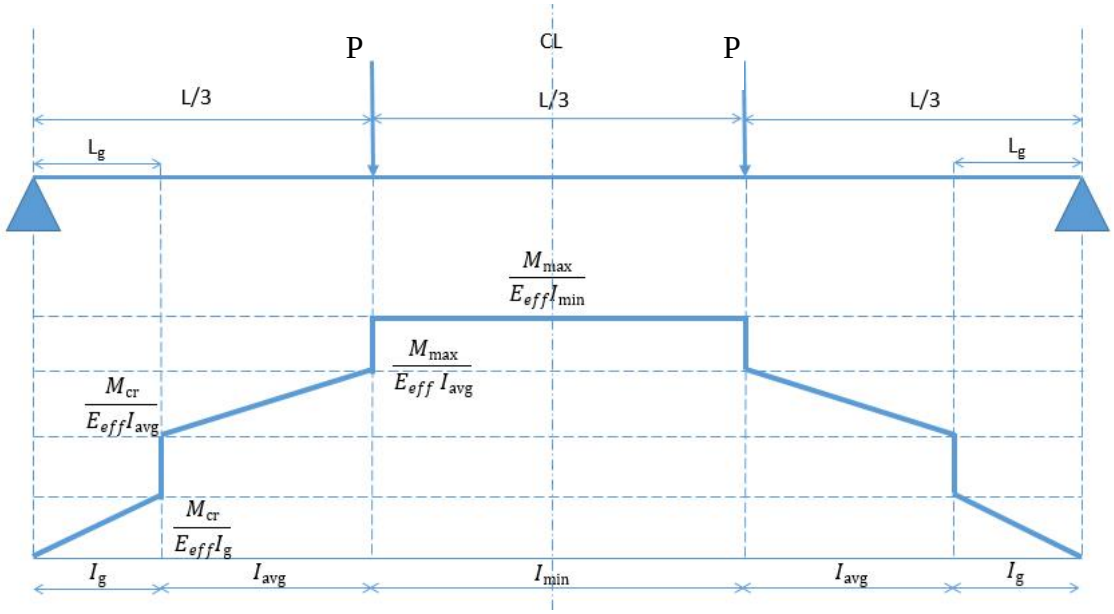


Figure 3.9: M/EI diagram for the verification experimental work

$$\delta_{max} = \frac{2\,M_{cr}}{E_{eff}\,I_g} * \frac{L_g}{2} * \left(0.5L - \frac{2L_g}{3}\right) + \frac{2\,M_{cr}}{E_{eff}\,I_{avg}}\left(\frac{L}{3} - L_g\right)\left\{\frac{L}{6} + \frac{1}{2}\left(\frac{L}{3} - L_g\right)\right\} + \left(\frac{M_{max}}{E_{eff}\,I_{avg}} - \frac{M_{cr}}{E_{eff}\,I_{avg}}\right) * \left(\frac{L}{3} - L_g\right) * \frac{2}{2} * \left\{\frac{L}{6} + \frac{1}{3}\left(\frac{L}{3} - L_g\right)\right\} + \frac{2\,M_{max}}{E_{eff}\,I_{min}}\left(\frac{L}{6} * \frac{L}{12}\right) \quad (3.6)$$

Where $L_g$ is the uncracked length of the beam which can be calculated as:

$$L_g = \frac{M_{cr}}{P} \tag{3.7}$$

The procedure is further illustrated in the flow chart of Figure 3.10:

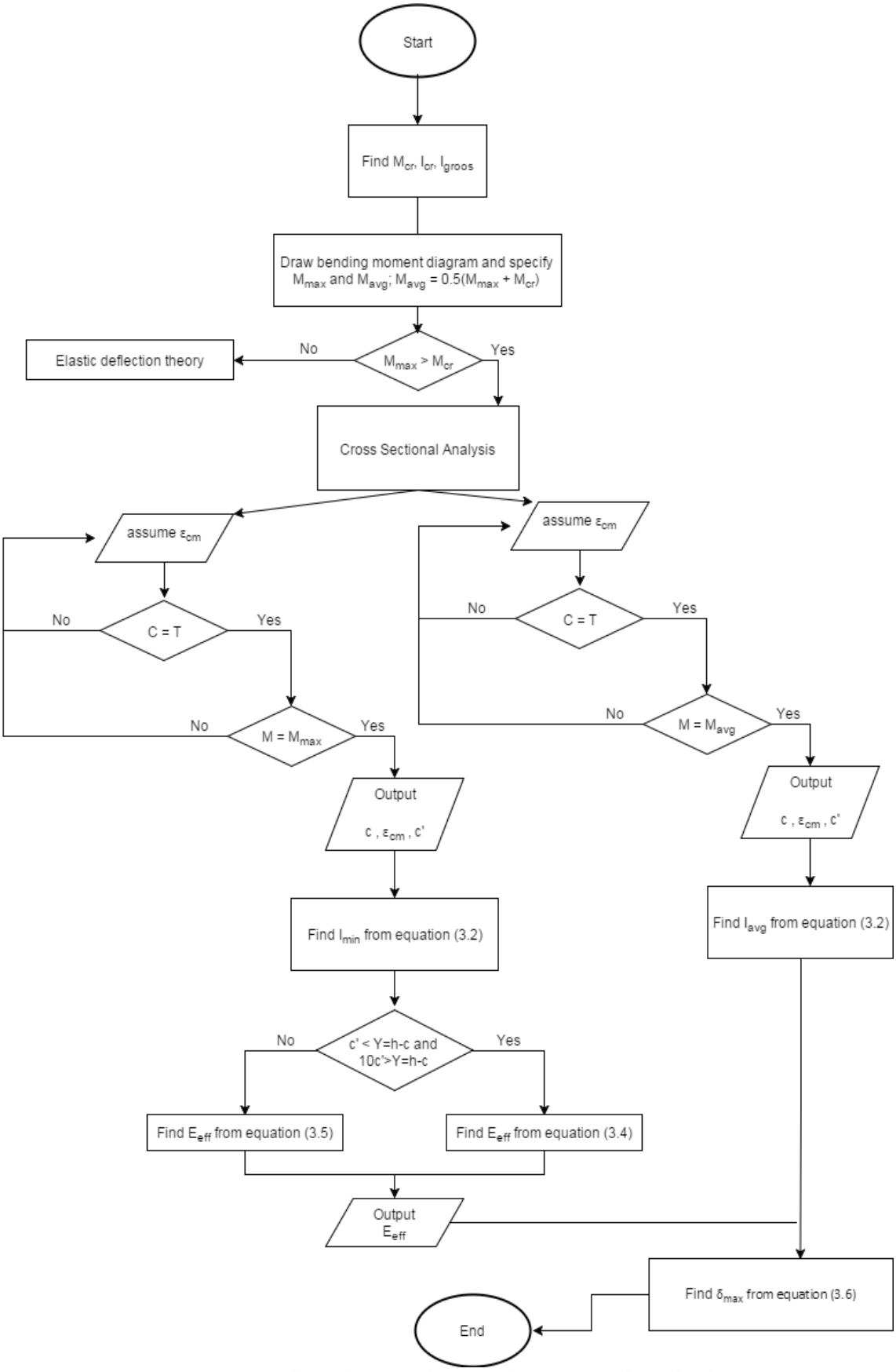


Figure 3.10: Flow chart explaining the proposed method

### 3.6.1 CSA S806-12 method (CSA, 2012)

Considering the case of four-point bending in Figure 3.11, the CSA S806 method, Originally derived by Razaqpur et al (Razaqpur, Svecova, & Cheung, 2000) specifies:

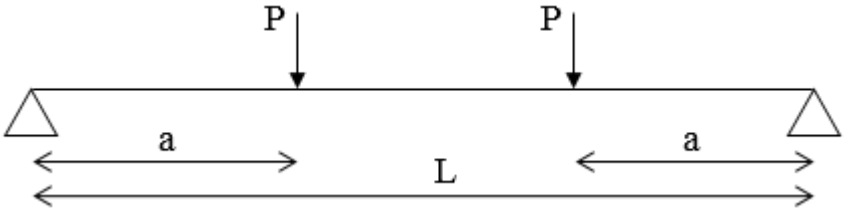


Figure 3.11: Four-point bending case

#### 3.6.1.1 Before cracking

Elastic theory and $I_{gross}$ are used.

$$\delta_{max} = \frac{P\,L^3}{6\,E_c\,I_g}\left[\frac{3a}{4L} - \left(\frac{a}{L}\right)^3\right] \tag{3.8}$$

$$\text{or} \quad \delta_{max} = \frac{23\,P\,L^3}{648\,E_c\,I_g}\;;\; a = \frac{L}{3} \tag{3.9}$$

#### 3.6.1.2 After cracking

The following formula is used:

$$\delta_{max} = \frac{P\,L^3}{24\,E_c\,I_{cr}}\left[3\left(\frac{a}{L}\right) - 4\left(\frac{a}{L}\right)^3 - 8\eta\left(\frac{L_g}{L}\right)^3\right] \tag{3.10}$$

Where: $\eta = \left(1 - \frac{I_{cr}}{I_g}\right)$

### 3.6.2 ACI Committee 440.1 R-06 method: (ACI, 2006)

This method is the modified Branson's method in which a correction factor $\beta_d$ is introduced to the formula. The original formula is given in Equation (2.8). Considering the same case of four-point bending, this method implies:

#### 3.6.2.1 Before cracking

Elastic theory and $I_{gross}$ are used.

$$\delta_{max} = \frac{P\,L^3}{6\,E_c\,I_g}\left[\frac{3a}{4L} - \left(\frac{a}{L}\right)^3\right] \quad (3.11)$$

$$\text{or} \quad \delta_{max} = \frac{23\,P\,L^3}{648\,E_c\,I_g}\;;\; a = \frac{L}{3} \quad (3.12)$$

### 3.6.2.2 After cracking

The same formula applies but $I_e$ is used instead of $I_{gross}$: based on ACI Committee 440.1 R-06, to find $I_e$ the following equations are used:

$$\rho_{f_b} = 0.85\,\beta_1\,\frac{f'_c}{f_{fu}}\,\frac{E_f\,\varepsilon_{cu}}{E_f\,\varepsilon_{cu} + f_{fu}} \quad (3.13)$$

where $\beta_1$ can be calculated from:

$$\beta_1 = \begin{cases} \beta_1 = 0.85\,;\, f'_c < 28\,MPa \\ \beta_1 = 0.85 - \frac{0.05}{7}\left(f'_c - 28\right)\;;\; f'_c > 28\,MPa \\ \beta_1 > 0.65\;\; \forall\, f'_c \end{cases} \quad (3.14)$$

$$I_e = \left(\frac{M_{cr}}{M_a}\right)^3 \beta_d\,I_g + \left[1 - \left(\frac{M_{cr}}{M_a}\right)^3\right] I_{cr} \;\leq\; I_g \quad (3.15)$$

where $\beta_d$ can be calculated from:

$$\beta_d = \frac{1}{5}\left(\frac{\rho_f}{\rho_{f_b}}\right) \leq 1.0 \quad (3.16)$$

And finally the deflection can be calculated using the following equation:

$$\delta max = \frac{P\,L^3}{6\,E_c\,I_e}\left[\frac{3a}{4L} - \left(\frac{a}{L}\right)^3\right] \quad (3.17)$$

$$\text{or} \quad \delta max = \frac{23\,P\,L^3}{648\,E_c\,I_e}\;;\; a = L/3 \quad (3.18)$$

In the next chapter the accuracy of these code methods for FRP reinforced concrete members will be compared with that of the proposed method over the entire loading range up to failure.

# Chapter 4

# VERIFICATION AND DISCUSSIONS

## 4.1 Introduction

This chapter includes the verification of the proposed method. This verification is conducted by comparing the results of the proposed method with the corresponding experimentally measured deflection values for seven beams. The tested beams vary in reinforcement ratio, width of the section, concrete class, and the concrete cover. Comparison is also made with the predictions of the ACI Committee 440.1 R-06 and CSA S806-12 methods. A brief explanation of the experimental work and test setups are also presented in this chapter. At the end, graphs are displayed to show the accuracy of the proposed method and discussion of the results is presented.

## 4.2 Experimental data

The data used for verifying the method was taken from three different published papers. (Barris, Torres, Comas, & Mias, 2013), (Barris, Torres, Turon, Baena, & Catalan, 2009), and (Qu, Zhang, & Huang, 2009). These data is based on experimental work in which the deflection under different stress level is reported. It is useful for verification as it compares different reinforcement ratios, width of the section, effective depth, and concrete strengths.

### 4.2.1 Test setups

According to the references (Barris et al., 2013) and (Barris et al., 2009), two specimens of each beam type have been tested. All of the tested beam were designed to fail by concrete crushing at the mid-span. The beam specimens had 2050 mm length,

rectangular cross-section with varied values of b, and a total depth of 190 mm. The span of the beams was 1800 mm, and distance between the applied loads was 600 mm. To assure that no shear failure will occur, the shear span was reinforced with transverse reinforcement of Φ8mm/70 mm and no transverse reinforcement provided in the pure bending zone. This was done to eliminate the possibility of getting influenced by the transverse reinforcement. The test setups can be illustrated in Figure 4.1.

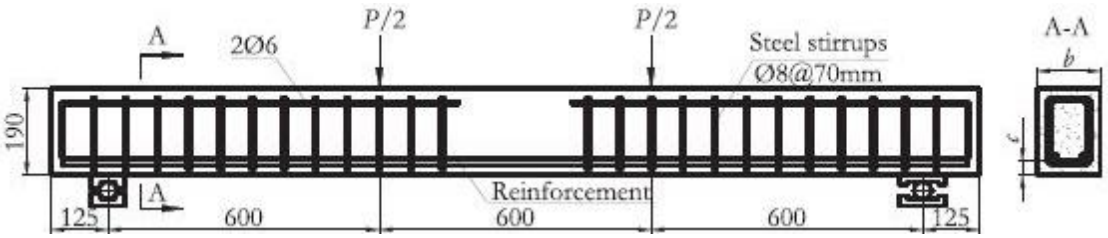

Figure 4.1: Test setups and details (mm) (Barris et al., 2013) (Barris et al., 2009)

All the beams were tested under a static four-point bending test. The load was applied by a servo-controlled hydraulic jack which had a capacity of 300 KN. The load from the jack was exerted on the beam by the mean of spreader steel beam. However, for the steel beam (B1) (Qu et al., 2009) it has the same span and the distance between applied loads. It has ductile behaviour. The depth of the section is 250 mm and the width 180 mm. As a transverse reinforcement, steel stirrups of Φ10mm/100 was applied outside the pure bending zone. Test setups and details for steel beam are shown in Figure 4.2.

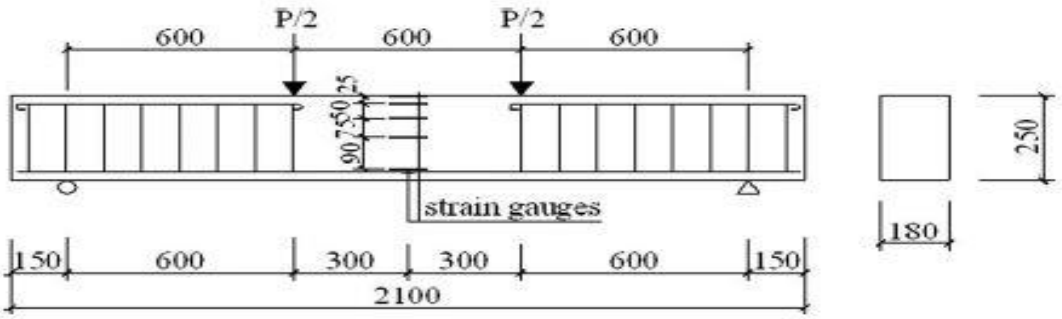

Figure 4.2: Shows the test setups and details for steel beam (Qu et al., 2009)

The geometrical information and the material properties of the tested beams are given in Table 4.1 and Table 4.2, respectively.

Table 4.1: Geometrical properties of the studied beams

| **Beam Name** | **Width b (mm)** | **Cover d' (mm)** | **Effective depth d (mm)** | **Rein.** | **ρ (%)** | **Concrete type** |
|---|---|---|---|---|---|---|
| N-212-D1* | 140 | 20 | 170 | 2φ12 | 0.99 | N |
| N-216-D1* | 140 | 20 | 170 | 2φ16 | 1.77 | N |
| N-316-D1* | 140 | 20 | 170 | 3φ16 | 2.66 | N |
| N-212-D2* | 160 | 40 | 150 | 2φ12 | 0.99 | N |
| C-216-D1** | 140 | 20 | 170 | 2φ16 | 1.78 | H |
| C-216-D2** | 160 | 40 | 150 | 2φ16 | 1.78 | H |
| H-316-D1* | 140 | 20 | 170 | 3φ16 | 2.66 | H |
| B1*** | 180 | 30 | 220 | 4φ12 | 1.14 | N |

* Cracking and deflection in GFRP RC beams: An experimental study. (Barris et al., 2013)
**An experimental study of the flexural behavior of GFRP RC beams and comparison with prediction models. (Barris et al., 2009)
*** Flexural Behavior of Concrete Beams Reinforced with Hybrid (GFRP and Steel) Bars(Qu et al., 2009)

Moreover, material properties of the studied beams are shown in Table 4.2 as follows:

Table 4.2: Material properties of the tested beams

| Beam Name | Concrete | | | Reinforcement bars | | |
|---|---|---|---|---|---|---|
| | $f'_c$ (MPa) | $f_{ct}$ (MPa) | $E_c$ (MPa) | $f_{fu}$ (MPa) | $E_f$ (MPa) | $\varepsilon_f$ (%) |
| N-212-D1 | 32.1 | 2.8 | 25,845 | 1321 | 63,437 | -1.8 |
| N-216-D1 | 32.1 | 2.8 | 25,845 | 1015 | 64,634 | -1.8 |
| N-316-D1 | 32.1 | 2.8 | 25,845 | 1015 | 64,634 | -1.8 |
| N-212-D2 | 32.1 | 2.8 | 25,845 | 1321 | 63,437 | -1.8 |
| C-216-D1 | 56.3 | 3.3 | 26,524 | 995 | 64,152 | -1.8 |
| C-216-D2 | 61.7 | 3.3 | 27318 | 995 | 64,152 | -1.8 |
| H-316-D1 | 54.5 | 4.1 | 28,491 | 1015 | 64,634 | -1.8 |
| B1 (steel reinforced) | 30.95 | 3.45 | 25,035 | $f_y$= 363 | 181,500 | $\varepsilon_y$ = 0. 2 |

## 4.3 Comparison between the proposed method results and experimental data

The results of the proposed method l are compared with the corresponding experimental data, and with the ACI Committee 440.1 R-06 method and CSA S806-12 methods predictions. The comparison is based on moment vs. deflection graphs. For each beam, two graphs are displayed. The first one shows the behaviour under serviceability loads (in the case of FRP, up to 40%$M_{ult}$ or in case of steel reinforcement, up to 50% $M_{ult}$) (Bischoff & Gross, 2011), the second one traces the full behaviour up to failure. A summary of the deflection values for several load levels is also presented in the table accompanying some of the moment-deflection Figures.

### 4.3.1 N-212-D1

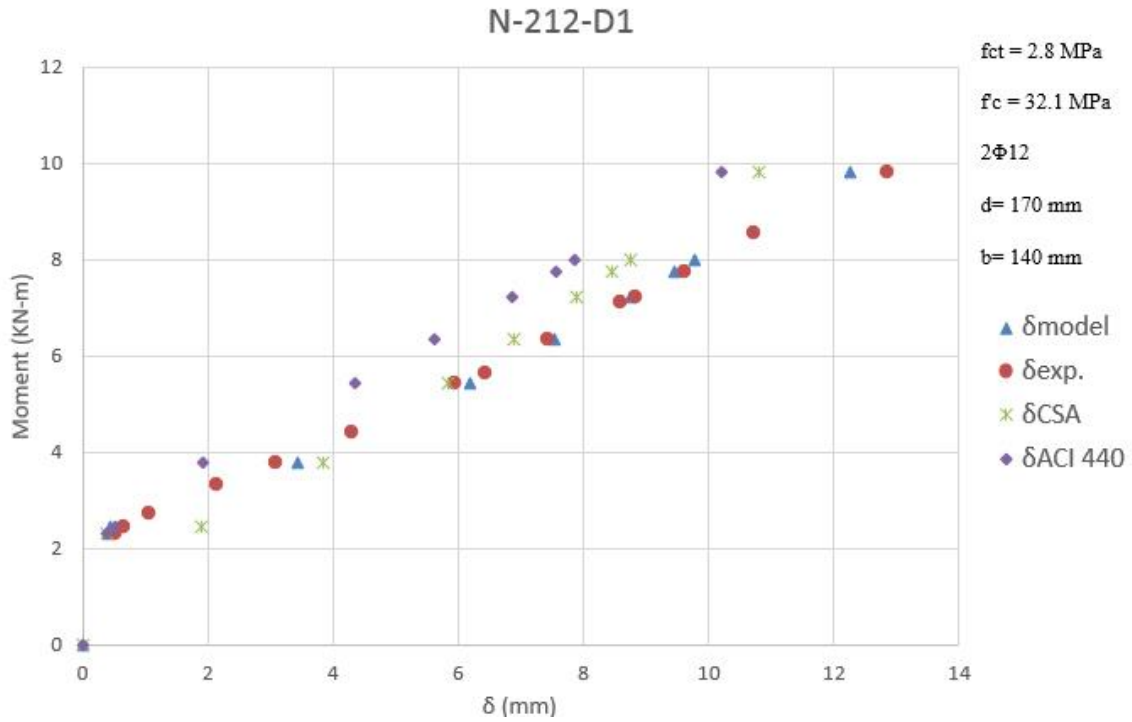


Figure 4.3: Beam N-212-D1 results within serviceability loads

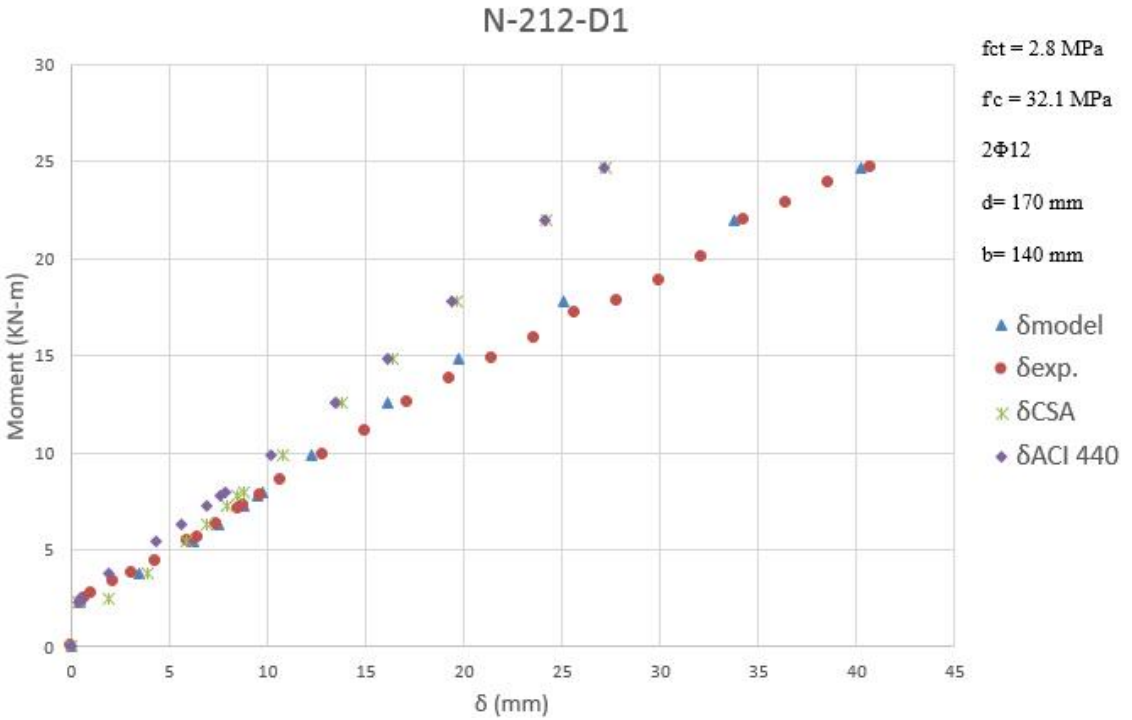


Figure 4.4: Beam N-212-D1 results of full behavior

Table 4.3: Ratios of applied methods under serviceability load - beam N-212-D1

| $M_{max}$ | $\delta_{exp.}$ | $\delta_{method}$ | $\delta_{method}/\delta_{exp.}$ | $\delta_{CSA}$ | $\delta_{CSA}/\delta_{exp.}$ | $\delta_{ACI\ 440}$ | $\delta_{ACI\ 440}/\delta_{exp.}$ |
|---|---|---|---|---|---|---|---|
| 3.78 | 3.084 | 3.437 | 1.114 | 3.839 | 1.245 | 1.941 | 0.630 |
| 5.45 | 5.942 | 6.200 | 1.043 | 5.854 | 0.985 | 4.347 | 0.732 |
| 6.35 | 7.416 | 7.525 | 1.015 | 6.883 | 0.928 | 5.633 | 0.760 |
| 7.24 | 8.832 | 8.749 | 0.991 | 7.897 | 0.894 | 6.866 | 0.777 |
| 7.75 | 9.626 | 9.437 | 0.980 | 8.471 | 0.880 | 7.545 | 0.784 |
| 9.84 | 12.857 | 12.261 | 0.954 | 10.804 | 0.840 | 10.189 | 0.792 |
| **Mean** | | | **1.016** | | **0.962** | | **0.746** |
| **Std. Deviation** | | | **0.057** | | **0.147** | | **0.061** |

Table 4.4: Ratios of applied methods under higher load levels - beam N-212-D1

| $M_{max}$ | $\delta_{exp.}$ | $\delta_{method}$ | $\delta_{method}/\delta_{exp.}$ | $\delta_{CSA}$ | $\delta_{CSA}/\delta_{exp.}$ | $\delta_{ACI\ 440}$ | $\delta_{ACI\ 440}/\delta_{exp.}$ |
|---|---|---|---|---|---|---|---|
| 12.56 | 17.143 | 16.116 | 0.940 | 13.825 | 0.806 | 13.434 | 0.784 |
| 14.86 | 21.429 | 19.703 | 0.919 | 16.373 | 0.764 | 16.091 | 0.751 |
| 17.79 | 27.857 | 25.053 | 0.899 | 19.612 | 0.704 | 19.414 | 0.697 |
| 21.98 | 34.286 | 33.748 | 0.984 | 24.236 | 0.707 | 24.105 | 0.703 |
| 24.70 | 40.714 | 40.250 | 0.989 | 27.240 | 0.669 | 27.136 | 0.666 |
| **Mean** | | | **0.946** | | **0.730** | | **0.720** |
| **Std. Deviation** | | | **0.039** | | **0.055** | | **0.047** |

### 4.3.2 N-216-D1

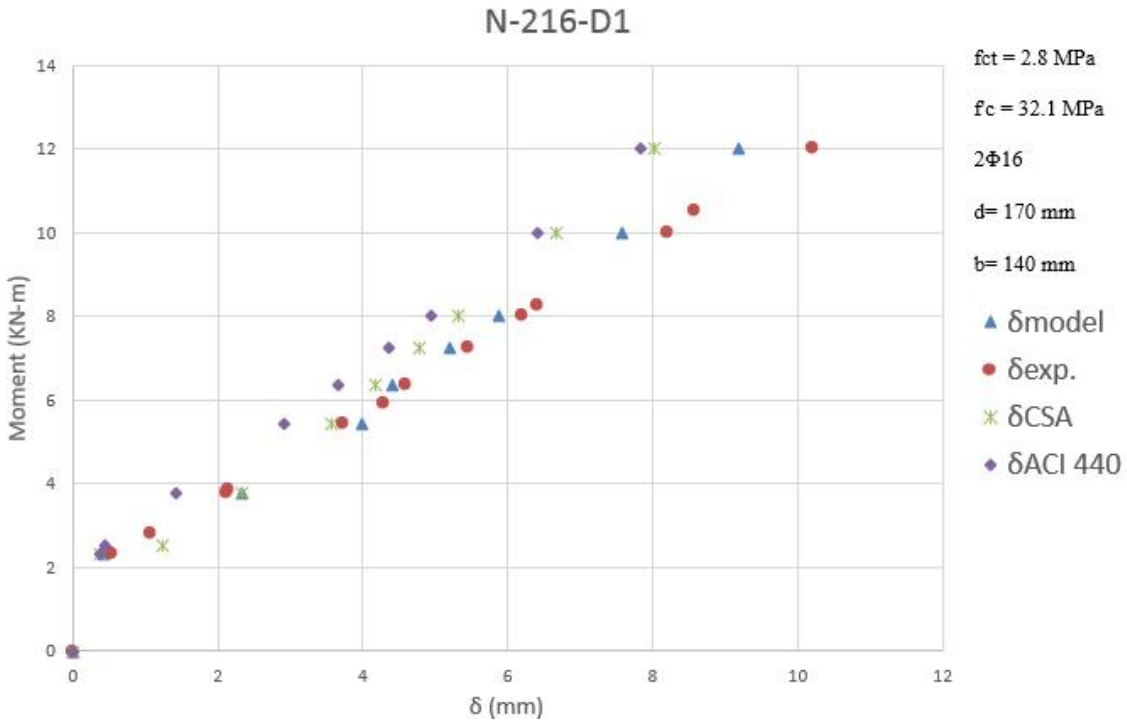


Figure 4.5: Beam N-216-D1 results within serviceability loads

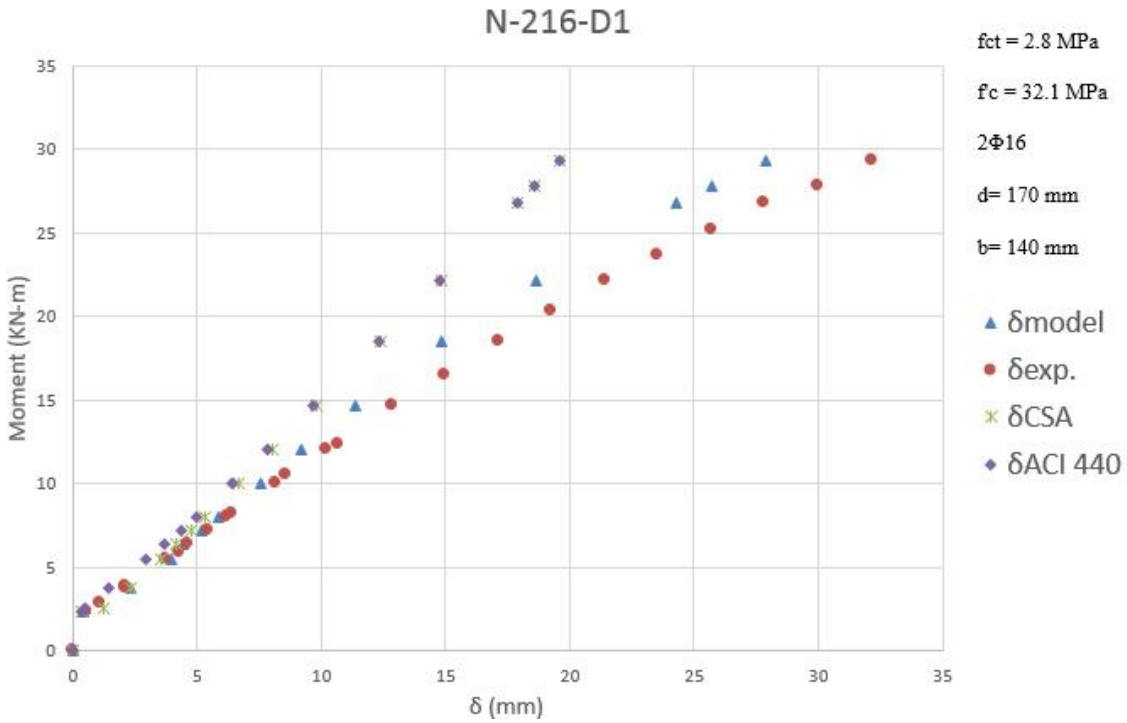


Figure 4.6: Beam N-216-D1 results of full behavior

Table 4.5: Ratios of applied methods under serviceability load - beam N-216-D1

| $M_{max}$ | $\delta_{exp.}$ | $\delta_{method}$ | $\delta_{method}/\delta_{exp.}$ | $\delta_{CSA}$ | $\delta_{CSA}/\delta_{exp.}$ | $\delta_{ACI\ 440}$ | $\delta_{ACI\ 440}/\delta_{exp.}$ |
|---|---|---|---|---|---|---|---|
| 3.78 | 2.113 | 2.336 | 1.106 | 2.337 | 1.106 | 1.426 | 0.675 |
| 5.45 | 3.726 | 3.976 | 1.067 | 3.556 | 0.954 | 2.900 | 0.778 |
| 6.35 | 4.601 | 4.405 | 0.957 | 4.180 | 0.908 | 3.651 | 0.793 |
| 7.24 | 5.471 | 5.193 | 0.949 | 4.795 | 0.876 | 4.367 | 0.798 |
| 8.00 | 6.218 | 5.869 | 0.944 | 5.314 | 0.855 | 4.952 | 0.796 |
| 10.00 | 8.199 | 7.575 | 0.924 | 6.669 | 0.813 | 6.427 | 0.784 |
| 12.00 | 10.203 | 9.183 | 0.900 | 8.016 | 0.786 | 7.846 | 0.769 |
| **Mean** | | | **0.978** | | **0.900** | | **0.771** |
| **Std. Deviation** | | | **0.071** | | **0.099** | | **0.040** |

Table 4.6: Ratios of applied methods under higher load levels - beam N-216-D1

| $M_{max}$ | $\delta_{exp.}$ | $\delta_{method}$ | $\delta_{method}/\delta_{exp.}$ | $\delta_{CSA}$ | $\delta_{CSA}/\delta_{exp.}$ | $\delta_{ACI\ 440}$ | $\delta_{ACI\ 440}/\delta_{exp.}$ |
|---|---|---|---|---|---|---|---|
| 14.66 | 12.857 | 11.365 | 0.884 | 9.802 | 0.762 | 9.686 | 0.753 |
| 18.51 | 17.143 | 14.818 | 0.864 | 12.390 | 0.723 | 12.316 | 0.718 |
| 22.11 | 21.429 | 18.632 | 0.869 | 14.803 | 0.691 | 14.751 | 0.688 |
| 26.74 | 27.857 | 24.314 | 0.873 | 17.904 | 0.643 | 17.869 | 0.641 |
| 27.77 | 30.000 | 25.692 | 0.856 | 18.593 | 0.620 | 18.560 | 0.619 |
| 29.31 | 32.143 | 27.862 | 0.867 | 19.626 | 0.611 | 19.597 | 0.610 |
| **Mean** | | | **0.869** | | **0.675** | | **0.672** |
| **Std. Deviation** | | | **0.009** | | **0.061** | | **0.058** |

### 4.3.3 N-316-D1

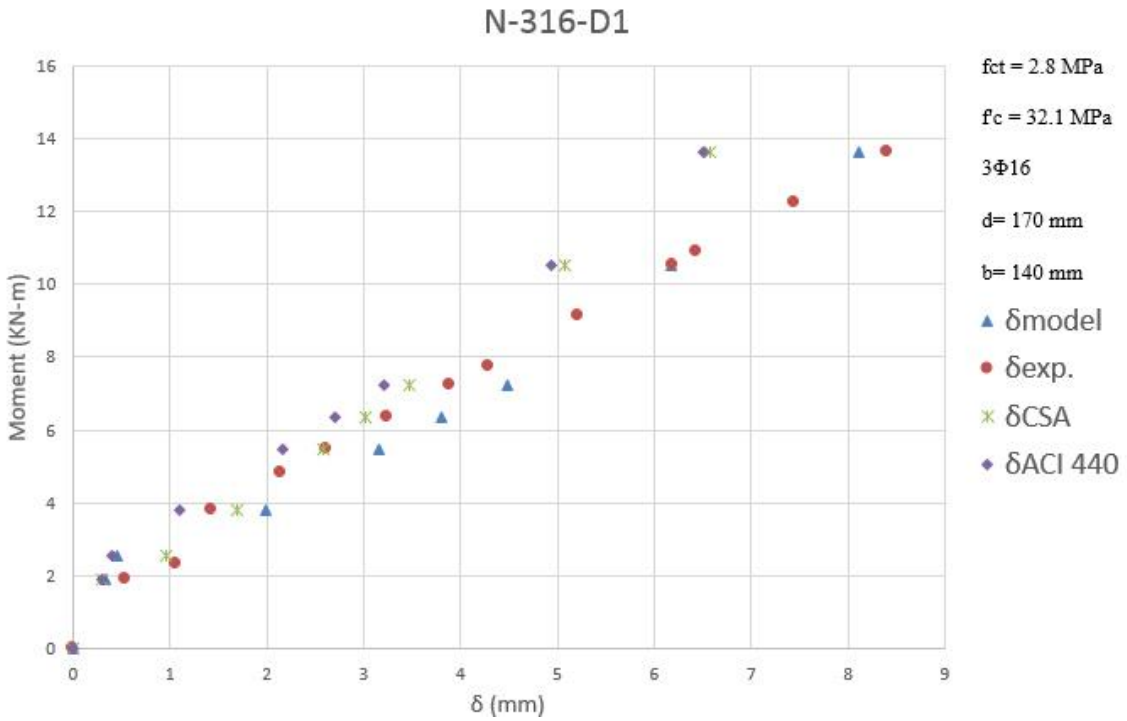


Figure 4.7: Beam N-316-D1 results within serviceability loads

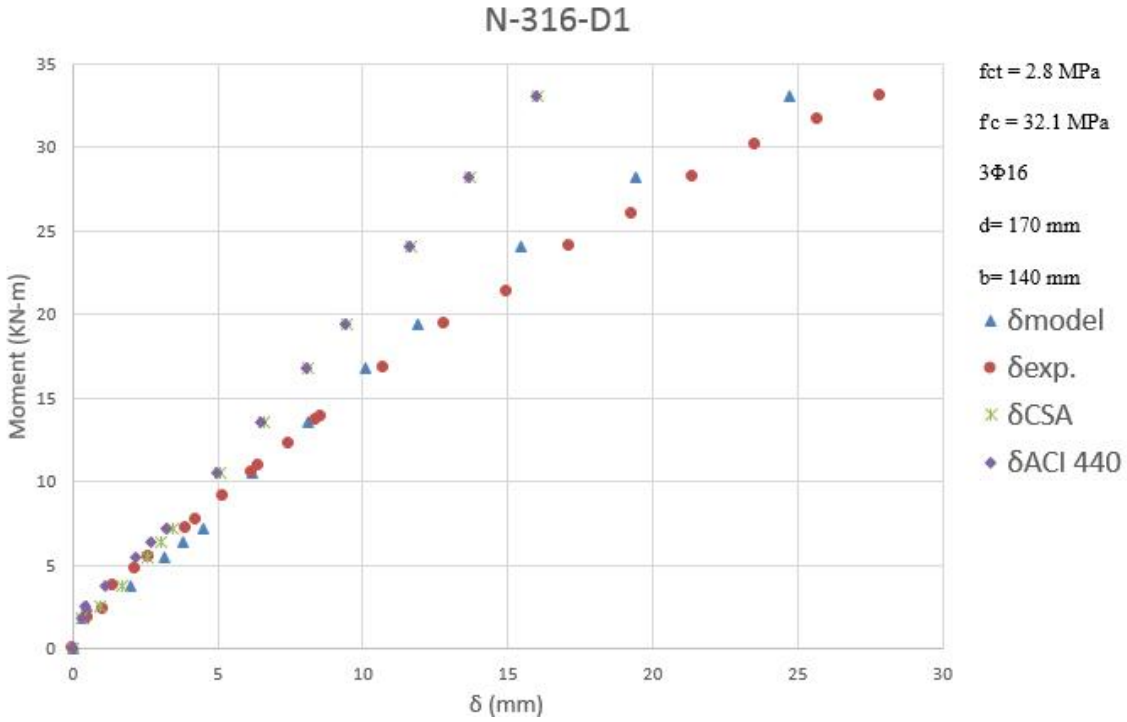


Figure 4.8: Beam N-316-D1 results of full behavior

Table 4.7: Ratios of applied methods under serviceability load - beam N-316-D1

| $M_{max}$ | $\delta_{exp.}$ | $\delta_{method}$ | $\delta_{method}/\delta_{exp.}$ | $\delta_{CSA}$ | $\delta_{CSA}/\delta_{exp.}$ | $\delta_{ACI\ 440}$ | $\delta_{ACI\ 440}/\delta_{exp.}$ |
|---|---|---|---|---|---|---|---|
| 3.78 | 1.423 | 1.998 | 1.404 | 1.695 | 1.191 | 1.106 | 0.777 |
| 5.45 | 2.61 | 3.153 | 1.208 | 2.574 | 0.986 | 2.166 | 0.830 |
| 6.35 | 3.25 | 3.810 | 1.172 | 3.025 | 0.931 | 2.699 | 0.831 |
| 7.24 | 3.883 | 4.476 | 1.153 | 3.469 | 0.893 | 3.207 | 0.826 |
| 10.50 | 6.2 | 6.174 | 0.996 | 5.067 | 0.817 | 4.934 | 0.796 |
| 13.61 | 8.412 | 8.113 | 0.964 | 6.579 | 0.782 | 6.499 | 0.773 |
| **Mean** | | | **1.150** | | **0.934** | | **0.805** |
| **Std. Deviation** | | | **0.159** | | **0.146** | | **0.027** |

Table 4.8: Ratios of applied method under higher load levels - beam N-316-D1

| $M_{max}$ | $\delta_{exp.}$ | $\delta_{method}$ | $\delta_{method}/\delta_{exp.}$ | $\delta_{CSA}$ | $\delta_{CSA}/\delta_{exp.}$ | $\delta_{ACI\ 440}$ | $\delta_{ACI\ 440}/\delta_{exp.}$ |
|---|---|---|---|---|---|---|---|
| 16.74 | 10.714 | 10.091 | 0.942 | 8.102 | 0.756 | 8.048 | 0.751 |
| 19.47 | 12.857 | 11.912 | 0.927 | 9.421 | 0.733 | 9.382 | 0.730 |
| 24.07 | 17.143 | 15.437 | 0.901 | 11.653 | 0.680 | 11.627 | 0.678 |
| 28.26 | 21.429 | 19.418 | 0.906 | 13.681 | 0.638 | 13.662 | 0.638 |
| 33.07 | 27.857 | 24.716 | 0.887 | 16.013 | 0.575 | 15.999 | 0.574 |
| **Mean** | | | **0.912** | | **0.676** | | **0.674** |
| **Std. Deviation** | | | **0.022** | | **0.073** | | **0.071** |

### 4.3.4 N-212-D2

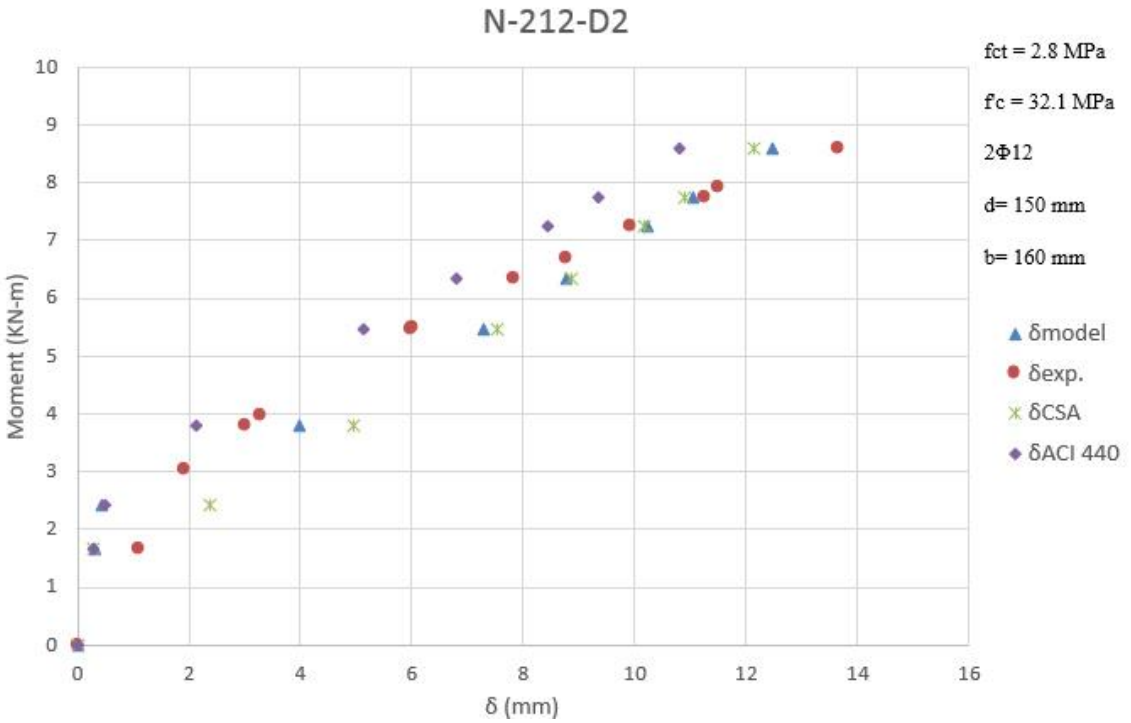


Figure 4.9: Beam N-212-D2 results within serviceability loads

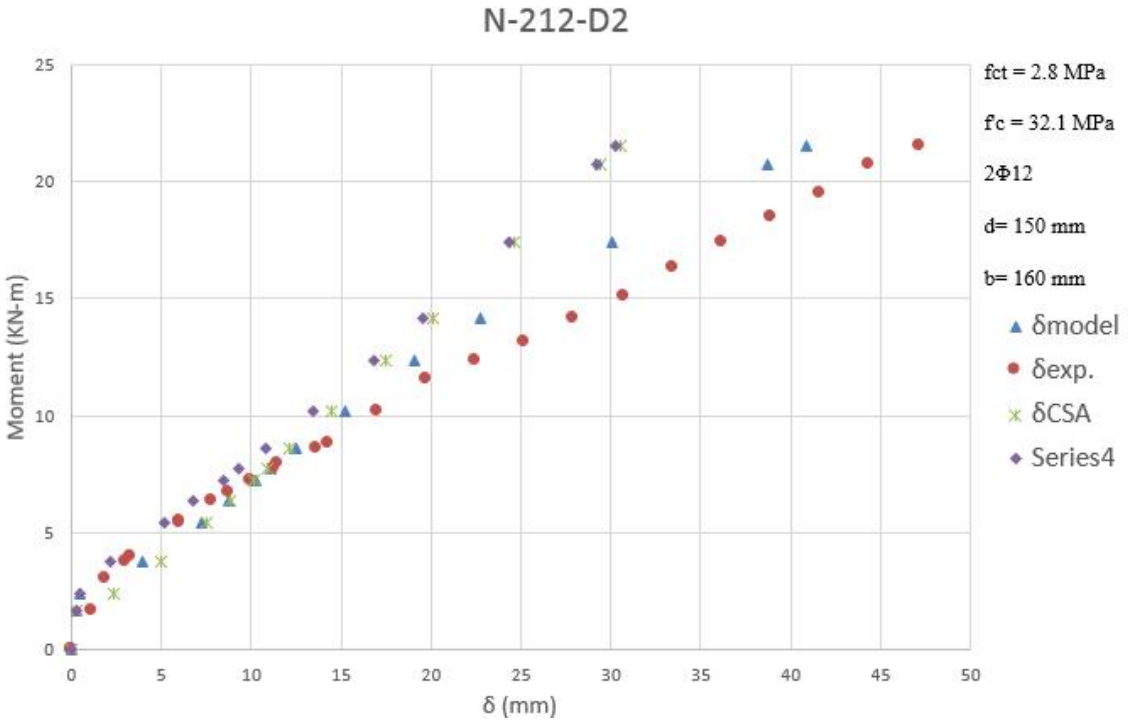


Figure 4.10: Beam N-212-D2 results full behavior

Table 4.9: Ratios of applied methods under serviceability load - beam N-212-D2

| $M_{max}$ | $\delta_{exp.}$ | $\delta_{method}$ | $\delta_{method}/\delta_{exp.}$ | $\delta_{CSA}$ | $\delta_{CSA}/\delta_{exp.}$ | $\delta_{ACI\ 440}$ | $\delta_{ACI\ 440}/\delta_{exp.}$ |
|---|---|---|---|---|---|---|---|
| 3.78 | 3.026 | 3.965 | 1.310 | 4.940 | 1.632 | 2.129 | 0.703 |
| 5.45 | 5.986 | 7.284 | 1.217 | 7.531 | 1.258 | 5.132 | 0.857 |
| 6.35 | 7.848 | 8.765 | 1.117 | 8.855 | 1.128 | 6.815 | 0.868 |
| 7.24 | 9.942 | 10.230 | 1.029 | 10.160 | 1.022 | 8.448 | 0.850 |
| 7.75 | 11.264 | 11.066 | 0.982 | 10.899 | 0.968 | 9.350 | 0.830 |
| 8.60 | 13.655 | 12.468 | 0.913 | 12.124 | 0.888 | 10.811 | 0.792 |
| **Mean** | | | **1.095** | | **1.149** | | **0.817** |
| **Std. Deviation** | | | **0.150** | | **0.270** | | **0.062** |

Table 4.10: Ratios of applied methods under higher load levels - beam N-212-D2

| $M_{max}$ | $\delta_{exp.}$ | $\delta_{method}$ | $\delta_{method}/\delta_{exp.}$ | $\delta_{CSA}$ | $\delta_{CSA}/\delta_{exp.}$ | $\delta_{ACI\ 440}$ | $\delta_{ACI\ 440}/\delta_{exp.}$ |
|---|---|---|---|---|---|---|---|
| 10.22 | 16.986 | 15.209 | 0.895 | 14.448 | 0.851 | 13.470 | 0.793 |
| 12.36 | 22.466 | 19.059 | 0.848 | 17.498 | 0.779 | 16.806 | 0.748 |
| 14.19 | 27.945 | 22.709 | 0.813 | 20.106 | 0.719 | 19.573 | 0.700 |
| 17.39 | 36.164 | 30.083 | 0.832 | 24.663 | 0.682 | 24.303 | 0.672 |
| 20.75 | 44.384 | 38.710 | 0.872 | 29.432 | 0.663 | 29.178 | 0.657 |
| 21.51 | 47.123 | 40.869 | 0.867 | 30.515 | 0.648 | 30.279 | 0.643 |
| **Mean** | | | **0.855** | | **0.724** | | **0.702** |
| **Std. Deviation** | | | **0.030** | | **0.078** | | **0.058** |

### 4.3.5 C-216-D1

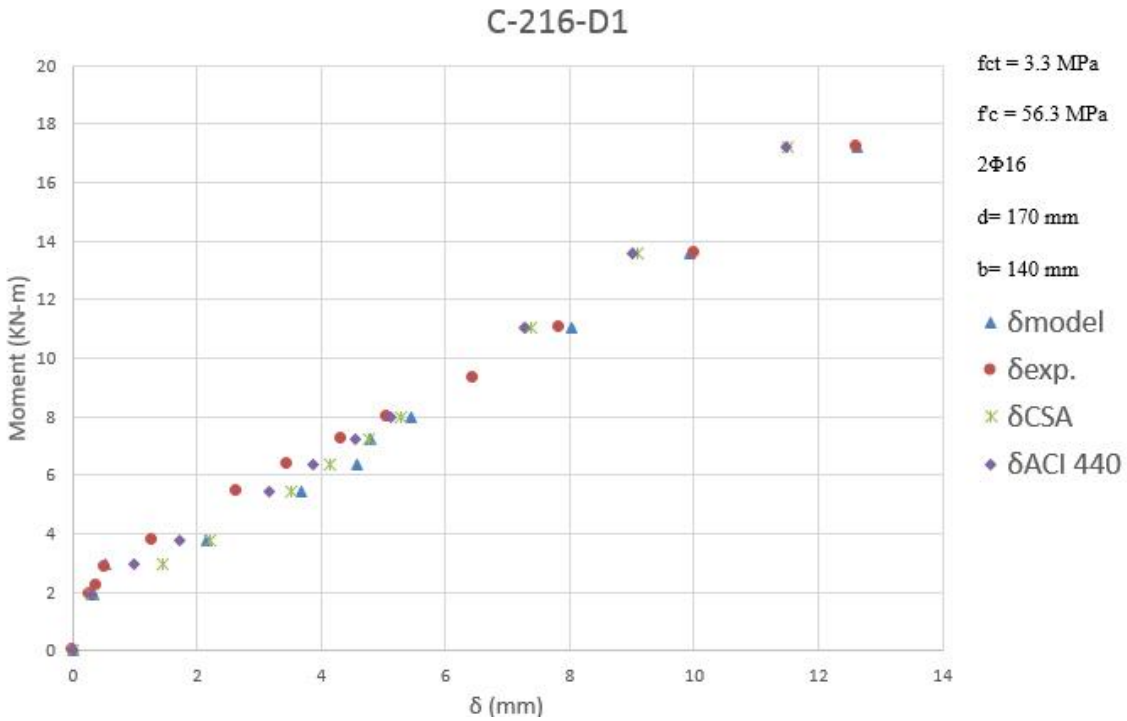


Figure 4.11: Beam C-216-D1 results within serviceability loads

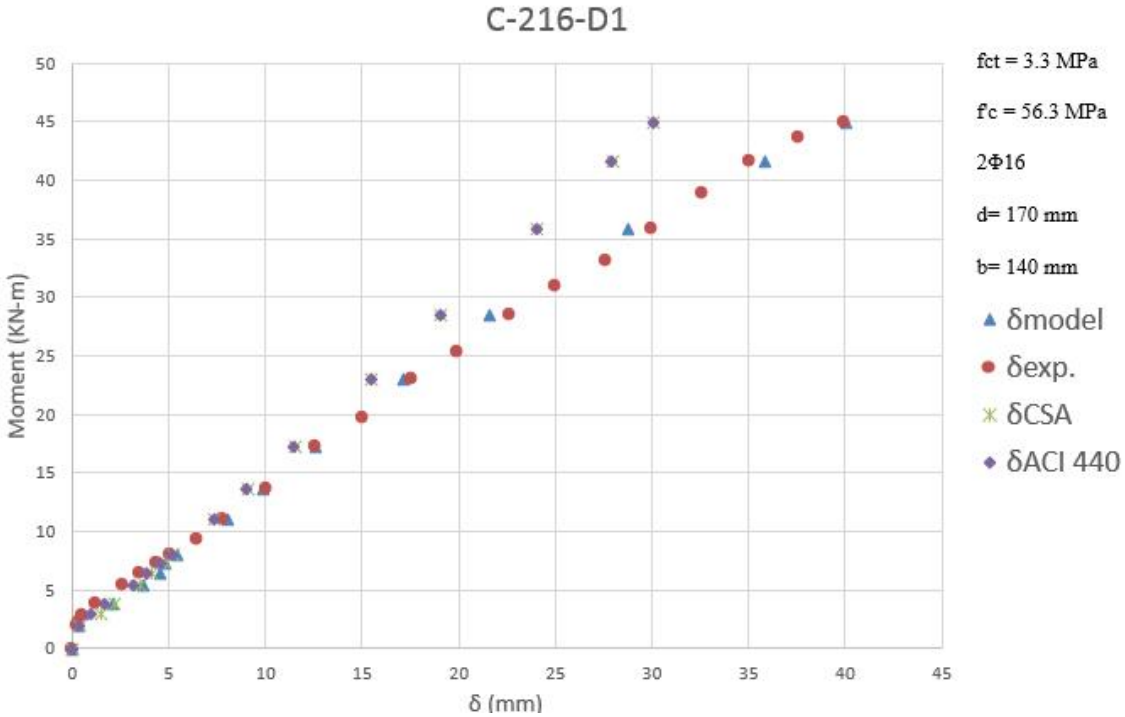


Figure 4.12: Beam C-216-D1 results of full behavior

Table 4.11: Ratios of applied methods under serviceability load - beam C-216-D1

| $M_{max}$ | $\delta_{exp.}$ | $\delta_{method}$ | $\delta_{method}/\delta_{exp.}$ | $\delta_{CSA}$ | $\delta_{CSA}/\delta_{exp.}$ | $\delta_{ACI\ 440}$ | $\delta_{ACI\ 440}/\delta_{exp.}$ |
|---|---|---|---|---|---|---|---|
| 3.78 | 1.277 | 2.146 | 1.680 | 2.217 | 1.736 | 1.720 | 1.347 |
| 5.45 | 2.636 | 3.686 | 1.399 | 3.501 | 1.328 | 3.156 | 1.197 |
| 6.35 | 3.457 | 4.584 | 1.326 | 4.141 | 1.198 | 3.867 | 1.119 |
| 7.24 | 4.329 | 4.783 | 1.105 | 4.767 | 1.101 | 4.547 | 1.050 |
| 8.00 | 5.058 | 5.437 | 1.075 | 5.292 | 1.046 | 5.108 | 1.010 |
| 11.05 | 7.827 | 8.017 | 1.024 | 7.372 | 0.942 | 7.272 | 0.929 |
| 13.58 | 10.017 | 9.926 | 0.991 | 9.078 | 0.906 | 9.011 | 0.900 |
| 17.21 | 12.632 | 12.618 | 0.999 | 11.522 | 0.912 | 11.480 | 0.909 |
| **Mean** | | | **1.268** | | **1.225** | | **1.109** |
| **Std. Deviation** | | | **0.250** | | **0.283** | | **0.148** |

Table 4.12: Ratios of applied methods under higher load levels – beam C-216-D1

| $M_{max}$ | $\delta_{exp.}$ | $\delta_{method}$ | $\delta_{method}/\delta_{exp.}$ | $\delta_{CSA}$ | $\delta_{CSA}/\delta_{exp.}$ | $\delta_{ACI\ 440}$ | $\delta_{ACI\ 440}/\delta_{exp.}$ |
|---|---|---|---|---|---|---|---|
| 23.05 | 17.632 | 17.093 | 0.969 | 15.445 | 0.876 | 15.421 | 0.875 |
| 28.42 | 22.632 | 21.562 | 0.953 | 19.047 | 0.842 | 19.031 | 0.841 |
| 35.84 | 30.000 | 28.749 | 0.958 | 24.023 | 0.801 | 24.014 | 0.800 |
| 41.68 | 35.000 | 35.794 | 1.023 | 27.941 | 0.798 | 27.933 | 0.798 |
| 44.84 | 40.000 | 40.063 | 1.002 | 30.058 | 0.751 | 30.052 | 0.751 |
| **Mean** | | | **0.981** | | **0.814** | | **0.813** |
| **Std. Deviation** | | | **0.030** | | **0.047** | | **0.047** |

### 4.3.6 C-216-D2

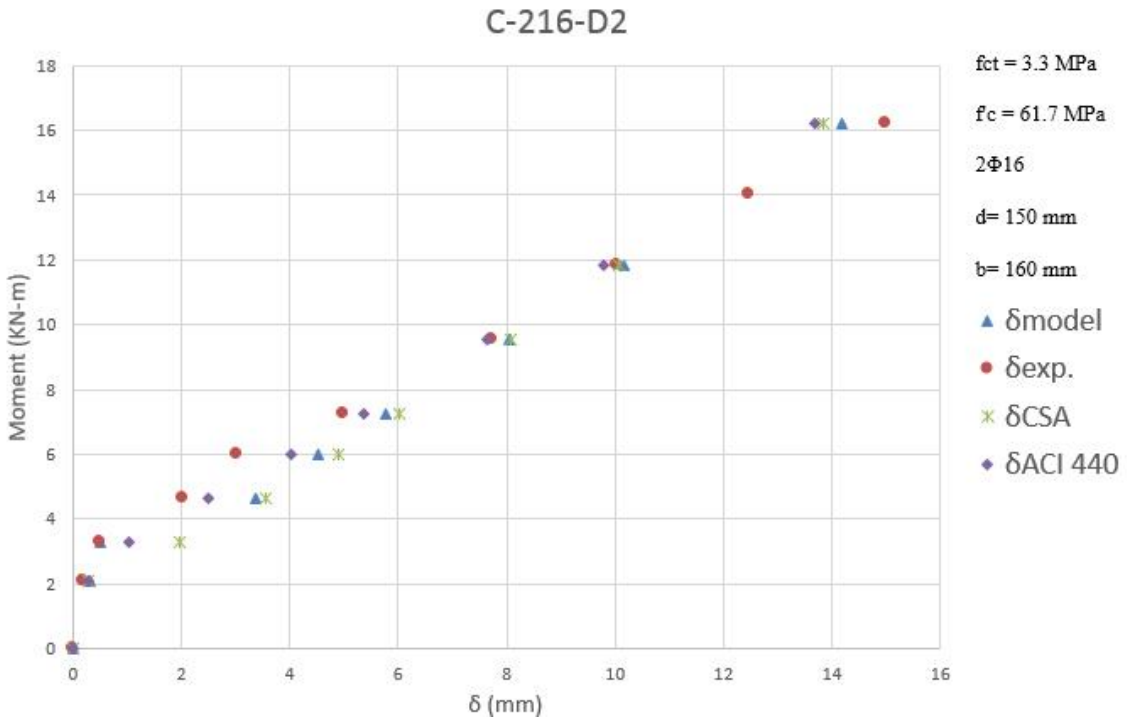


Figure 4.13: Beam C-216-D2 results within serviceability loads

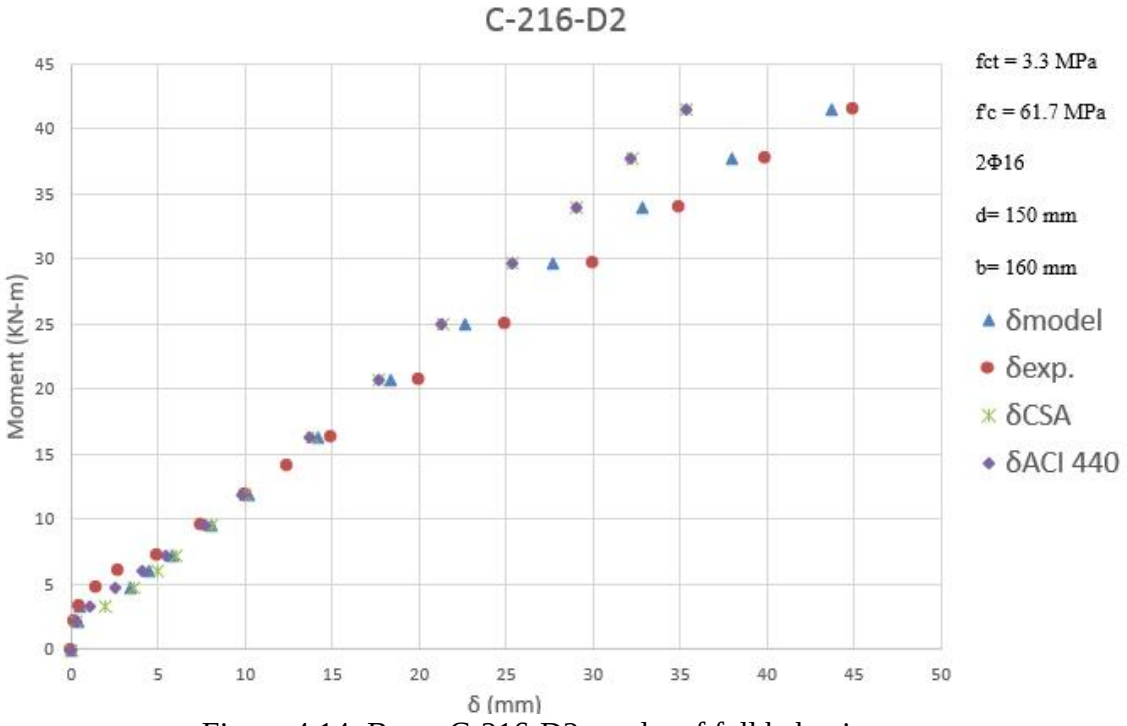


Figure 4.14: Beam C-216-D2 results of full behavior

Table 4.13: Ratios of applied methods under serviceability load - beam C-216-D2

| $M_{max}$ | $\delta_{exp.}$ | $\delta_{method}$ | $\delta_{method}/\delta_{exp.}$ | $\delta_{CSA}$ | $\delta_{CSA}/\delta_{exp.}$ | $\delta_{ACI\ 440}$ | $\delta_{ACI\ 440}/\delta_{exp.}$ |
|---|---|---|---|---|---|---|---|
| 4.64 | 2.031 | 3.372 | 1.661 | 3.559 | 1.752 | 2.498 | 1.230 |
| 6.00 | 3.041 | 4.526 | 1.488 | 4.890 | 1.608 | 4.039 | 1.328 |
| 7.23 | 5 | 5.770 | 1.154 | 6.018 | 1.204 | 5.356 | 1.071 |
| 9.54 | 7.74 | 8.055 | 1.041 | 8.064 | 1.042 | 7.646 | 0.988 |
| 11.85 | 10.054 | 10.172 | 1.012 | 10.074 | 1.002 | 9.792 | 0.974 |
| 16.23 | 15 | 14.178 | 0.945 | 13.850 | 0.923 | 13.695 | 0.913 |
| **Mean** | | | **1.217** | | **1.255** | | **1.084** |
| **Std. Deviation** | | | **0.290** | | **0.345** | | **0.162** |

Table 4.14: Ratios of applied methods under higher load levels - beam C-216-D2

| $M_{max}$ | $\delta_{exp.}$ | $\delta_{method}$ | $\delta_{method}/\delta_{exp.}$ | $\delta_{CSA}$ | $\delta_{CSA}/\delta_{exp.}$ | $\delta_{ACI\ 440}$ | $\delta_{ACI\ 440}/\delta_{exp.}$ |
|---|---|---|---|---|---|---|---|
| 20.73 | 20.000 | 18.370 | 0.918 | 17.712 | 0.886 | 17.616 | 0.881 |
| 24.99 | 25.000 | 22.576 | 0.903 | 21.362 | 0.854 | 21.296 | 0.852 |
| 29.73 | 30.000 | 27.680 | 0.923 | 25.420 | 0.847 | 25.374 | 0.846 |
| 34.02 | 35.000 | 32.869 | 0.939 | 29.092 | 0.831 | 29.057 | 0.830 |
| 37.71 | 40.000 | 37.998 | 0.950 | 32.250 | 0.806 | 32.221 | 0.806 |
| 41.43 | 45.000 | 43.750 | 0.972 | 35.433 | 0.787 | 35.409 | 0.787 |
| **Mean** | | | **0.927** | | **0.845** | | **0.843** |
| **Std. Deviation** | | | **0.018** | | **0.029** | | **0.028** |

### 4.3.7 H-316-D1

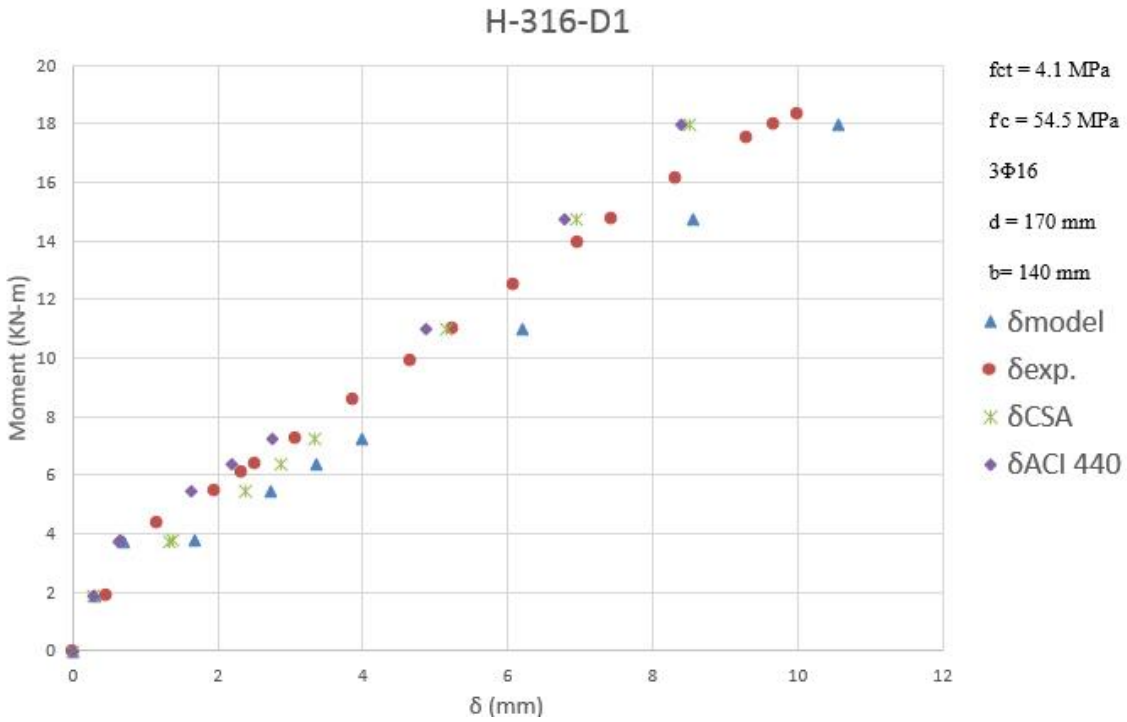


Figure 4.15: Beam H-316-D1 results within serviceability loads

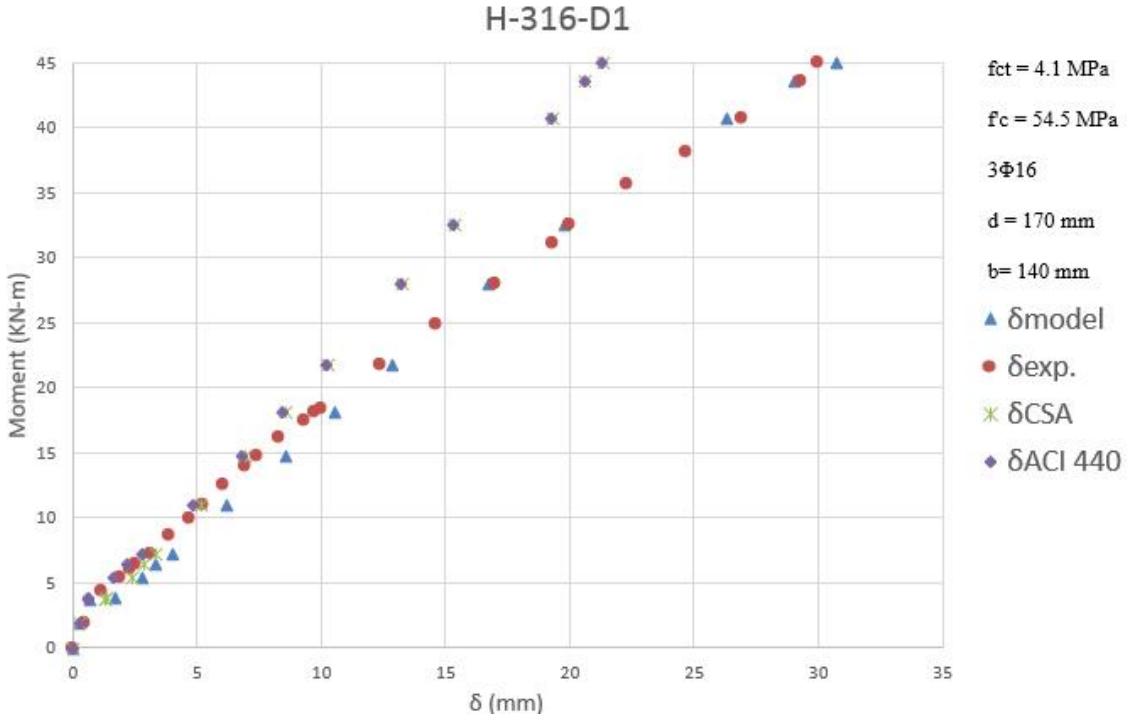


Figure 4.16: Beam H-316-D1 results full behavior

Table 4.15: Ratios of applied methods under serviceability load - beam H-316-D1

| $M_{max}$ | $\delta_{exp.}$ | $\delta_{method}$ | $\delta_{method}/\delta_{exp.}$ | $\delta_{CSA}$ | $\delta_{CSA}/\delta_{exp.}$ | $\delta_{ACI\ 440}$ | $\delta_{ACI\ 440}/\delta_{exp.}$ |
|---|---|---|---|---|---|---|---|
| 5.45 | 1.94 | 2.744 | 1.414 | 2.386 | 1.230 | 1.635 | 0.843 |
| 6.35 | 2.527 | 3.344 | 1.323 | 2.863 | 1.133 | 2.199 | 0.870 |
| 7.24 | 3.079 | 3.982 | 1.293 | 3.321 | 1.079 | 2.751 | 0.894 |
| 10.99 | 5.248 | 6.196 | 1.181 | 5.163 | 0.984 | 4.866 | 0.927 |
| 14.74 | 7.431 | 8.552 | 1.151 | 6.962 | 0.937 | 6.790 | 0.914 |
| 18.00 | 9.696 | 10.573 | 1.090 | 8.519 | 0.879 | 8.401 | 0.866 |
| **Mean** | | | **1.272** | | **1.072** | | **0.889** |
| **Std. Deviation** | | | **0.108** | | **0.117** | | **0.034** |

Table 4.16: Ratios of applied methods under higher load levels - beam H-316-D1

| $M_{max}$ | $\delta_{exp.}$ | $\delta_{method}$ | $\delta_{method}/\delta_{exp.}$ | $\delta_{CSA}$ | $\delta_{CSA}/\delta_{exp.}$ | $\delta_{ACI\ 440}$ | $\delta_{ACI\ 440}/\delta_{exp.}$ |
|---|---|---|---|---|---|---|---|
| 21.72 | 12.326 | 12.826 | 1.041 | 10.290 | 0.835 | 10.209 | 0.828 |
| 27.93 | 16.977 | 16.711 | 0.984 | 13.239 | 0.780 | 13.190 | 0.777 |
| 32.43 | 20.000 | 19.768 | 0.988 | 15.375 | 0.769 | 15.339 | 0.767 |
| 40.66 | 26.977 | 26.333 | 0.976 | 19.278 | 0.715 | 19.254 | 0.714 |
| 43.45 | 29.302 | 29.053 | 0.991 | 20.603 | 0.703 | 20.582 | 0.702 |
| 45.00 | 30.000 | 30.697 | 1.023 | 21.339 | 0.711 | 21.320 | 0.711 |
| **Mean** | | | **0.996** | | **0.760** | | **0.758** |
| **Std. Deviation** | | | **0.025** | | **0.053** | | **0.051** |

### 4.3.8 B1

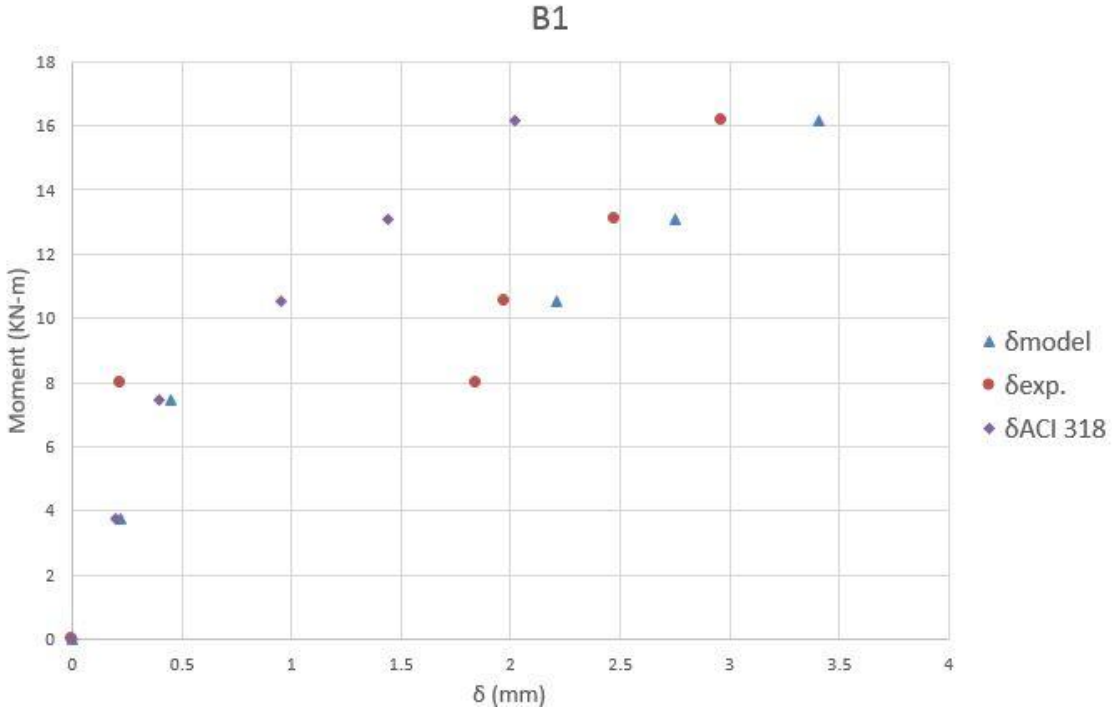


Figure 4.17: Beam B1 results within serviceability loads

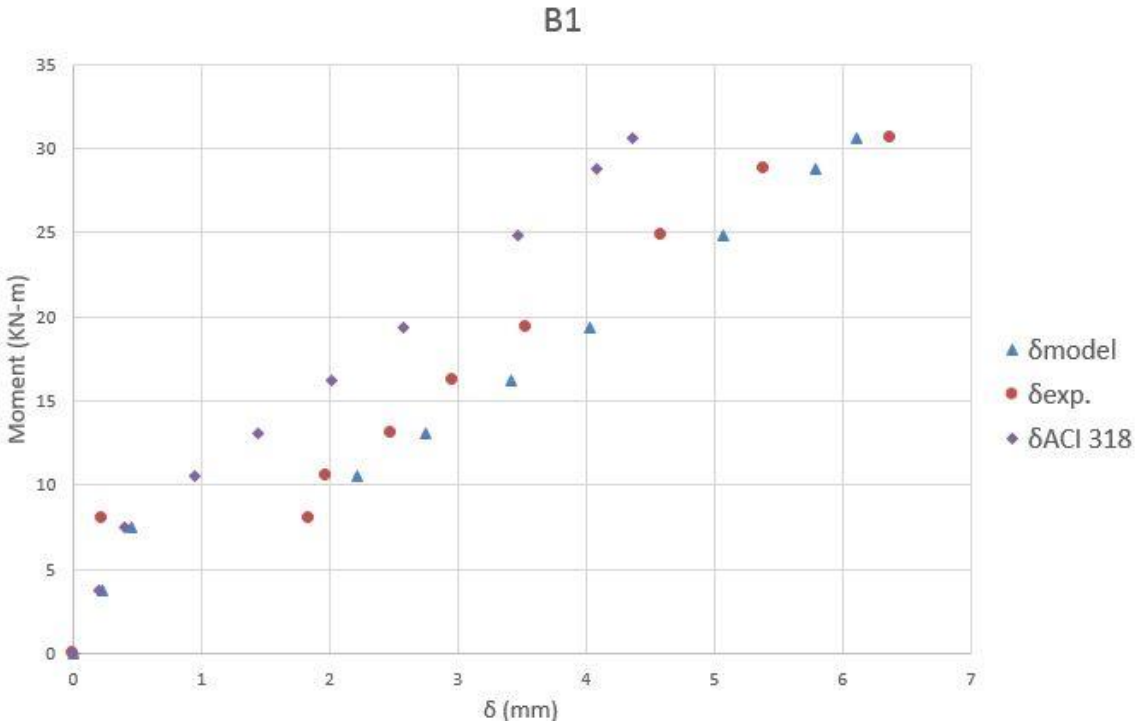


Figure 4.18: Beam B1 results full behavior

Table 4.17: Ratios of applied methods under serviceability load - beam B1

| $M_{max}$ | $\delta_{exp.}$ | $\delta_{method}$ | $\delta_{method}/\delta_{exp.}$ | $\delta_{ACI\ 318}$ | $\delta_{ACI\ 318}/\delta_{exp.}$ |
|---|---|---|---|---|---|
| 10.53 | 1.98 | 2.212 | 1.118 | 0.949 | 0.480 |
| 13.07 | 2.48 | 2.748 | 1.109 | 1.442 | 0.582 |
| 16.18 | 2.967 | 3.410 | 1.149 | 2.021 | 0.681 |
| **Mean** | | | **1.126** | | **0.581** |
| **Std. Deviation** | | | **0.021** | | **0.101** |

Table 4.18: Ratios of applied methods under higher load levels - beam B1

| $M_{max}$ | $\delta_{exp.}$ | $\delta_{method}$ | $\delta_{method}/\delta_{exp.}$ | $\delta_{ACI\ 318}$ | $\delta_{ACI\ 318}/\delta_{exp.}$ |
|---|---|---|---|---|---|
| 19.33 | 3.533 | 4.032 | 1.141 | 2.569 | 0.727 |
| 24.84 | 4.589 | 5.063 | 1.103 | 3.469 | 0.756 |
| 28.79 | 5.389 | 5.783 | 1.073 | 4.087 | 0.758 |
| 30.58 | 6.378 | 6.107 | 0.958 | 4.362 | 0.684 |
| **Mean** | | | **1.069** | | **0.731** |
| **Std. Deviation** | | | **0.079** | | **0.035** |

## 4.4 Discussion of results

### 4.4.1 Discussing the FRP reinforced beams case

Considering the full behaviour, the proposed method gives reasonable and better results than both the ACI and CSA methods. However, it overestimates the deflection at the serviceability load level. According to the verification of the proposed method, it overestimates the deflection at the serviceability limit state of high strength concrete beams with bigger ratio (average ratio 1.252) than for normal strength concrete (average ratio 1.06) as shown in Table 4.19. However, CSA method gives better results for normal strength concrete at the serviceability limit state (average ratio 0.986) but for high strength concrete, the ACI method gives better estimation (average ratio 1.027) as explained in Table 4.19. Still the proposed method gives acceptable results at the serviceability limit state.

Concerning the higher load levels, which has limitations for most of deflection formula, the proposed method gives closer results to experimental results for both high and normal strength concrete compared to ACI and CSA methods. This is demonstrated in Table 4.20. The proposed method l gives better results for high strength concrete (average ratio 0.968) comparing to normal strength concrete (average ratio 0.896).

Comparing the standard deviation of the ratios of different methods, it can be noticed that for serviceability loads, the ACI Committee 440 method has the lowest average standard deviation values as shown in Table 4.21. For the case of higher load levels, the proposed method has the lowest average standard deviation values as displayed in Table 4.22. It should be kept in mind that the lower the standard deviation value, the less difference exists between the individual ratios and the average value of these ratios. This means predicting the deflection with almost the same accuracy.

Table 4.19: Comparing the ratios of the applied methods for serviceability loads of FRP reinforced beams

| **Beam name** | **Serviceability** | | |
|---|---|---|---|
| | **Average** $\delta_{method}/\delta_{exp.}$ | **Average** $\delta_{CSA}/\delta_{exp.}$ | **Average** $\delta_{ACI\ 440}/\delta_{exp.}$ |
| N-212-D1 | 1.016 | 0.962 | 0.746 |
| N-216-D1 | 0.978 | 0.900 | 0.771 |
| N-316-D1 | 1.150 | 0.934 | 0.805 |
| N-212-D2 | 1.095 | 1.149 | 0.817 |
| **Average** | **1.060** | **0.986** | **0.785** |
| C-216-D1 | 1.268 | 1.225 | 1.109 |
| C-216-D2 | 1.217 | 1.255 | 1.084 |
| H-316-D1 | 1.272 | 1.072 | 0.889 |
| **Average** | **1.252** | **1.184** | **1.027** |

Table 4.20: Comparing the ratios of the applied methods for higher load levels of FRP reinforced beams

| Beam name | Higher load levels | | |
|---|---|---|---|
| | **Average** $\delta_{method}/\delta_{exp.}$ | **Average** $\delta_{CSA}/\delta_{exp.}$ | **Average** $\delta_{ACI\ 440}/\delta_{exp.}$ |
| N-212-D1 | 0.946 | 0.730 | 0.720 |
| N-216-D1 | 0.869 | 0.675 | 0.672 |
| N-316-D1 | 0.912 | 0.676 | 0.674 |
| N-212-D2 | 0.855 | 0.724 | 0.702 |
| **Average** | **0.896** | **0.701** | **0.692** |
| C-216-D1 | 0.981 | 0.814 | 0.813 |
| C-216-D2 | 0.927 | 0.845 | 0.843 |
| H-316-D1 | 0.996 | 0.760 | 0.758 |
| **Average** | **0.968** | **0.806** | **0.805** |

Table 4.21: Comparing standard deviation of the applied methods for serviceability loads of FRP reinforced beams

| Beam name | Serviceability | | |
|---|---|---|---|
| | **Standard dev.** $\delta_{method}/\delta_{exp.}$ | **Standard dev.** $\delta_{CSA}/\delta_{exp.}$ | **Standard dev.** $\delta_{ACI\ 440}/\delta_{exp.}$ |
| N-212-D1 | 0.057 | 0.147 | 0.061 |
| N-216-D1 | 0.071 | 0.099 | 0.040 |
| N-316-D1 | 0.159 | 0.146 | 0.027 |
| N-212-D2 | 0.150 | 0.270 | 0.062 |
| **Average** | **0.109** | **0.166** | **0.048** |
| C-216-D1 | 0.250 | 0.283 | 0.148 |
| C-216-D2 | 0.290 | 0.345 | 0.162 |
| H-316-D1 | 0.108 | 0.117 | 0.034 |
| **Average** | **0.216** | **0.265** | **0.119** |

Table 4.22: Comparing the standard deviation of the applied methods for higher load of FRP reinforced beams levels

| Beam name | Higher load levels | | |
|---|---|---|---|
| | **Standard dev.** $\delta_{method}/\delta_{exp.}$ | **Standard dev.** $\delta_{CSA}/\delta_{exp.}$ | **Standard dev.** $\delta_{ACI\ 440}/\delta_{exp.}$ |
| N-212-D1 | 0.039 | 0.055 | 0.047 |
| N-216-D1 | 0.009 | 0.061 | 0.058 |
| N-316-D1 | 0.022 | 0.073 | 0.071 |
| N-212-D2 | 0.030 | 0.078 | 0.058 |
| **Average** | **0.025** | **0.067** | **0.059** |
| C-216-D1 | 0.030 | 0.047 | 0.047 |
| C-216-D2 | 0.018 | 0.029 | 0.028 |
| H-316-D1 | 0.025 | 0.053 | 0.051 |
| **Average** | **0.024** | **0.043** | **0.042** |

### 4.4.2 Discussing steel reinforced beam case

The proposed method gave reasonable results in the full behaviour. Considering the serviceability limits, the proposed method overestimated the deflection (average ratio 1.126) as mentioned in Table 4.17. Considering the higher load levels, the proposed method overestimated the deflection too but with a smaller average ratio (1.069) which is demonstrated in Table 4.18. Comparing these average ratios with ACI Committee 318 and the experimental work, the proposed method gives reliable results and better estimation. However, the tested steel reinforced beam is ductile beam (under reinforced) and the concrete type is normal strength, that is why further investigation is required to verify this method completely for steel reinforced beams use, and this is out of this research scoop.

# Chapter 5

# CONCLUSION

The concept of tension stiffening has significant effect on the deflection of steel reinforced concrete members, but for FRP reinforced concrete members some researchers have stated that it is less important.

The ACI Committee 440 deflection calculation method for FRP reinforced concrete beams accounts for tension stiffening while the Canadian CSA S806-12 method ignores it, yet both give relatively reliable results under service load. But both underestimates the deflection significantly for higher load levels. According to these codes, their suggested expressions are only intended for service load conditions, which is verified by the current results.

The experimental work used for verification gives good variation of conditions in which the reinforcement ratio, effective depth, width of section, concrete class, elastic modulus, and FRP properties are varied to ascertain the reliability of the proposed method.

In the case of FRP reinforced concrete beams, the proposed method overestimated deflection under the serviceability conditions, and underestimated deflection for higher load levels. However, the results are still reliable.

In the case of FRP reinforced concrete beams, considering serviceability loads, the proposed method gives more reliable results for normal strength concrete compared to high strength concrete. This could be due to the constitutive law of concrete under compression.

The proposed method gives acceptable results for serviceability limits but using CSA S806-12 method for normal strength concrete and ACI Committee 440 method for high strength concrete is preferred. This conclusion is based on comparing the results of the studied experimental work.

On the other hand, for the case of higher load levels FRP reinforced concrete beams, the proposed method gives closer results to experimental work for the case of high strength concrete rather than normal strength concrete. Using the proposed method rather than ACI Committee 440 or CSA S806-12 methods is advised for the case of higher load levels.

The proposed method overestimated deflection for steel reinforced beam under serviceability and higher load levels. Comparing the results to ACI Committee 318, the application of the proposed method is preferred for all the load levels. However, further verification of the proposed method is required for steel reinforced beams.

**Recommendations for Future Work**

(1) The proposed method is aimed at short-term deflection calculation, but it can be extended to long-term deflection calculation by considering the creep transformed section concept in conjunction with incremental analysis.

(2) Extend the method to other loading and boundary conditions, including beams with applied end moments as well as loads along the member.

(3) Apply more refined constitutive laws for concrete to better represent the behavior of different concrete strengths.

(4) Study the sensitivity of the method results to the tension-stiffening model and its parameters

# REFERENCES


ACI. (2006). *ACI 440.1R-06: Guide for the Design and Construction of Structural Concrete Reinforced with FRP Bars* (pp. 44): ACI.

Aron, M. & Chee Yee, K. (2006). Design criteria for bi-stable behavior in a buckled multi-layered MEMS bridge. *Journal of Micromechanics and Microengineering, 16*(10), 2034.

CSA. (2012). *S806-12 - Design and construction of building structures with fibre-reinforced polymers* (pp. 206): CSA.

Barris, C., Torres, L., Comas, J., & Mias, C. (2013). Cracking and deflections in GFRP RC beams: An experimental study. *Composites Part B-Engineering, 55*, 580-590. doi:10.1016/j.compositesb.2013.07.019

Barris, C., Torres, L., Turon, A., Baena, M., & Catalan, A. (2009). An experimental study of the flexural behaviour of GFRP RC beams and comparison with prediction models. *Composite Structures, 91*(3), 286-295. doi: 10.1016/j.compstruct.2009.05.005

Bažant, Z. P., & Cedolin, L. (1991). *Stability of Structures: Elastic, Inelastic, Fracture, and Damage Theories*: Dover Publications.

Bischoff, P. H., & Gross, S. P. (2011). Equivalent Moment of Inertia Based on Integration of Curvature. *Journal of Composites for Construction, 15*(3), 263-273. doi:10.1061/(ASCE)cc.1943-5614.0000164

Fabbrocino, G., Manfredi, G., & Cosenza, E. (2000). Analysis of continuous composite beams including partial interaction and bond. *Journal of Structural Engineering-Asce, 126*(11), 1288-1294. doi:10.1061/(asce)0733-9445(2000)126:11(1288)

Gar, S. P., Head, M., & Hurlebaus, S. (2012). Tension Stiffening in Prestressed Concrete Beams Using Moment-Curvature Relationship. *Journal of Structural Engineering-Asce, 138*(8), 1075-1078. doi:10.1061/(asce)st.1943-541x.0000534

Gilbert, R. I. (2007). Tension stiffening in lightly reinforced concrete slabs. *Journal of Structural Engineering-ASCE, 133*(6), 899-903. doi:10.1061/(ASCE)0733-9445(2007)133:6(899)

Haskett, M., Oehlers, D. J., Ali, M. S. M., & Wu, C. Q. (2009). Yield Penetration Hinge Rotation in Reinforced Concrete Beams. *Journal of Structural Engineering-ASCE, 135*(2), 130-138. doi:10.1061/(asce)0733-9445(2009)135:2(130)

Koppitz, R., Kenel, A., & Keller, T. (2014). Tension Chord Model Modification for Uniaxial Unloading and Reloading in Elastic and Plastic States (vol 140,

04014077, 2014). *Journal of Structural Engineering, 140*(10), 2. doi:10.1061/(ASCE)st.1943-541x.0001142

Park, R., & Paulay, T. (1975). *Reinforced Concrete Structures*: Wiley.

Popove, E. P., T. A. (1998). *Engineering Mechanics of Solids (2nd Edition)*. N.J: Prentice Hall.

Qu, W. J., Zhang, X. L., & Huang, H. Q. (2009). Flexural Behavior of Concrete Beams Reinforced with Hybrid (GFRP and Steel) Bars. *Journal of Composites for Construction, 13*(5), 350-359. doi:10.1061/(ASCE)cc.1943-5614.0000035

Razaqpur, A. G., Svecova, D., & Cheung, M. S. (2000). Rational method for calculating deflection of fiber-reinforced polymer reinforced beams. *ACI Structural Journal, 97*(1), 175-184.

Scott, R. H., & Beeby, A. W. (2005). Long-term tension-stiffening effects in concrete. *ACI Structural Journal, 102*(1), 31-39.

Stramandinoli, R. S. B., & La Rovere, H. L. (2008). An efficient tension-stiffening model for nonlinear analysis of reinforced concrete members. *Engineering Structures, 30*(7), 2069-2080. doi:10.1016/j.engstruct.2007.12.022

Taylor, P. J. (1970). Initial and Long-Term Deflections of a Reinforced Concrete Flat Plate Structure (Vol. CE12, pp. 14-22): *Civil Engineering Transactions (Sydney)*.

Zanuy, C., de la Fuente, P., & Albajar, L. (2010). Estimation of parameters defining negative tension stiffening. *Engineering Structures, 32*(10), 3355-3362. doi:10.1016/j.engstruct.2010.07.009

# APPENDIX

# Appendix A: User manual of using the working excel files

The related excel files are attached in the CD. There are two files, the first one "General cross sectional analysis" which does the cross sectional analysis to find c and $\varepsilon_{cm}$, the second file "General Beam deflection" is to calculate I, $E_{eff}$, and $\delta_{max}$. Moreover, a sample containing solution for beam N-212-D1 is included in the CD too.

The process of calculating the deflection is demonstrated in Figure 3.10.

1. Open "General Beam deflection" file and fill the input part in "Section properties" tab.

   N.B. Don't ever change the value of cells highlighted in grey.

   In "General Beam deflection" file, go to "Deflection calculation" sheet and fill the cells highlighted in light green. You can fill the cells depending on your need. To fill the light green cells related to each load case, you need to choose maximum moment corresponding to each loading case, then you should use the "General cross sectional analysis" file.

   N.B. Don't ever change the value of cells highlighted in grey.

2. To find the depth of neutral axis "c" and corresponding maximum compression strain in concrete" $\varepsilon_{cm}$", the "General cross sectional analysis" file is used. When you open this file, there is single sheet. Fill the values of section and material properties in the first row of the table, it will be automatically replicated other the entire table. To make the iteration process easier, macro has been included in this excel file so make sure to enable the macro when you open the file. After filling all the properties, start assuming value for $\varepsilon_{cm}$. To

find the corresponding resistant moment, click on the corresponding "C-T" cell in the same row, and launch the iteration process by clicking on "Ctrl+g". The value of the highlighted cell "C-T" will turn into zero, and you can read the resistant moment from the corresponding cell in the same row. Repeat this process until you reach your target moment.

3. Copy the value of "c" and "$\varepsilon_{cm}$" to the corresponding light green cells in the "General Beam deflection" file, in "Deflection calculation" tab.
4. Repeat the same process for $M_{avg}$ following steps 3 and 4.
5. After filling the corresponding cells, the values of moment of inertia and effective elastic modulus will be calculated considering the procedure explained in the proposed method part. Finally, the deflection is calculated.
6. Repeat this process until you calculate the deflection for the corresponding load level cases.
7. Summary of deflection output from the proposed method, CSA S806-12, and ACI Committee 440 methods are mentioned in "Deflection output" sheet.
8. Graphical output can be also generated in "Full behaviour chart" sheet. It compares the predicted deflection of proposed method, CSA S806-12, and ACI Committee 440 methods.
9. If the file will be used to compare the output of the methods with experimental data, the experimental data can be entered in "Experimental beam" sheet, and it will be included in the graphs automatically.
10. Lastly, if comparison with experimental data is required, "Comparison" sheet can be used which compares the output of the deflection of proposed method, CSA S806-12, and ACI Committee 440 methods with experimental data.

It should be noted that the excel files are prepared for four-point-bending beams with bottom reinforcement only. Double reinforced beams are not included. However, the case of double reinforced FRP reinforced beams are not common.